SIZING AND CONTROL OF FLYWHEEL ENERGY STORAGE FOR RAMEA WIND-HYDROGEN-DIESEL HYBRID POWER SYSTEM

KHADEMUL ISLAM

SIZING AND CONTROL OF FLYWHEEL ENERGY STORAGE FOR RAMEA WIND-HYDROGEN-DIESEL HYBRID POWER SYSTEM

BY

KHADEMUL ISLAM © B.Sc. Eng.

A thesis submitted to the School of Graduate Studies in partial fulfillment of the requirements for the degree of Master of Engineering

Faculty of Engineering & Applied Science

Memorial University of Newfoundland

April 2011

St. John's, Newfoundland, Canada

Abstract

In this thesis, a flywheel energy storage system (FESS) is proposed for the isolated wind-hydrogen-diesel hybrid power system in Ramea, Newfoundland, Canada. Sizing and control of the flywheel energy storage for Ramea wind-hydrogen-diesel hybrid power system is presented. At present, the hybrid power system in Ramea consists of diesel generators, wind turbines, hydrogen generator and Electrolyzer. The main objective of this proposed flywheel energy storage system is to minimize sudden variations of grid voltage and frequency due to variable wind speed and variable load. HOMER software is used for sizing and steady-state simulations, while MATLAB/Simulink is used for modeling and dynamic analysis of Ramea Hybrid power system. The selected size of the FESS is tested experimentally using a setup which is composed of 2kW DC machine based flywheel energy storage. The test DC machine is used as a motor/generator unit coupled with a cast steel flywheel rotor, a programmable data acquisition card, two controllable power supply units, two electromechanical relays and relay driving circuits. Steady state simulation shows that the addition of a flywheel energy storage to Ramea system will reduces the fuel consumption by the diesel generator, reduces the excess electrical energy per year, increases the renewable penetration to the grid and reduces the number of starting the diesel generator per year. These observations can be advantageous in prolonging the life span of the diesel generator, as well as reducing its maintenance. Also the observations indicate that the voltage on the grid-side can stabilized under frequency dynamic variation.

Acknowledgements

Table of Contents

List of Figures

List of Tables

Glossary

List of Symbols

A_{SA}	Swept area covered by the turbine rotor in m^2
C_p	Power coefficient
P_{ro}	Turbine rotor output from the wind in W
v_w	Wind velocity in m/s
R_t	Radius of turbine rotor
β	Pitch angle of rotor blades in degree
λ	Tip speed ratio

λ_i	Intermediate variable to calculate tip speed ratio
ρ	Air density in kg/m^3
ω_m	Angular velocity of turbine rotor rad/s
r_s	Stator winding resistance
r_r'	Rotor winding resistance
L_{ls}, L_{lr}'	Leakage inductance of stator and stator winding
L_m	Magnetizing inductance
L_{ed}, L_{eq}	Equivalent inductance in d and q- axes, respectively
V_{ds}, V_{qs}	d and q components of stator voltage
V_{dr}', V_{qr}'	d and q components of rotor voltage
i_{ds}, i_{qs}	d and q components of stator current
i_{dr}', i_{qr}'	d and q components of rotor current
$\varphi_{ds}, \varphi_{qs}$	d and q components of stator flux linkage
$\varphi_{dr}', \varphi_{qr}'$	d and q components of rotor flux linkage
$\varphi_{md}, \varphi_{mq}$	d and q components of mutual flux linkage
ω_e	Speed of the synchronously rotating reference frame
ω_r	Electrical angular speed of the rotor
ω_{rm_IM}	Mechanical angular speed of the induction motor rotor
θ_r	Electrical angular position of the rotor

θ_{rm_IM}	Mechanical angular position of the induction motor rotor
p_{WG}	Number of poles pair of wind generator
T_{em_IM}	Electromagnetic torque developed by induction motor
T_{m_WT}	Mechanical torque of wind turbine
J_{WG}	Inertia co-efficient for wind generator
F_{WG}	Friction co-efficient for wind generator
V_{dr}, V_{qr}	Corrected d and q component rotor voltage of rotor side converter
V'_{d_cor}, V'_{q_cor}	Correction factor for d and q component rotor voltage of rotor side converter
r_{ss}	Synchronous machine stator winding resistance
r'_{fd}	d-axis field winding resistance
r'_{kd}	d-axis damper winding resistance
r'_{kq1}	q-axis first damper winding resistance
r'_{kq2}	q-axis second damper winding resistance
L_{lss}	Leakage inductance of the synchronous machine stator winding
L'_{lfd}	Leakage inductance of the d-axis field winding
L'_{lkd}	Leakage inductance of the d-axis damper winding
L'_{lkq1}	Leakage inductance of the q-axis first damper winding
L'_{lkq2}	Leakage inductance of the q-axis second damper winding

L_{md}	d-axis magnetizing inductance
L_{mq}	q-axis magnetizing inductance
L_d	d-axis combined inductance of leakage and magnetizing component
L_q	q-axis combined inductance of leakage and magnetizing component
L_{eqd}, L_{eqq}	Total equivalent inductance in d and q- axes, respectively
V_d, V_q	d and q axis stator voltage component of synchronous machine
V'_{fd}	d-axis field voltage component
V'_{kd}	d-axis damper winding voltage
V'_{kq1}	q-axis first damper winding voltage
V'_{kq2}	q-axis second damper winding voltage
i_d, i_q	d and q axis current component of synchronous motor stator
i'_{fd}	d-axis field current
i'_{kd}	d-axis damper winding current
i'_{kq1}	q-axis first damper winding current
i'_{kq2}	q-axis second damper winding current
φ_d	Stator d-axis flux linkage component
φ_q	Stator q-axis flux linkage component
φ'_{fd}	d-axis field winding flux linkage
φ'_{kd}	d-axis damper winding flux linkage

φ'_{kq1}	q-axis first damper winding flux linkage
φ'_{kq2}	q-axis second damper winding flux linkage
φ_{mds}	d-axis mutual flux linkage
φ_{mqs}	q-axis mutual flux linkage
ω_r	Electrical angular speed of the rotor
ω_{rm_SM}	Mechanical angular speed of the synchronous motor rotor
θ_r	Electrical angular position of the rotor
θ_{rm_SM}	Mechanical angular position of the synchronous motor rotor
p_{SM}	Number of pole pairs of synchronous motor
T_{em_SM}	Electromagnetic torque of Synchronous motor
T_m	Mechanical torque
J_{SM}	Inertia co-efficient of synchronous machine
F_{SM}	Friction co-efficient of synchronous machine
q	Turbine flow rate
H_0	Water column static head
H	Head at the turbine inlet
H_L	Head loss due to friction
g	Acceleration
A_{pen}	Cross sectional area of the penstock
L	Length of the penstock

$\overline{q}$	Turbine flow rate in per unit
$\overline{G}$	Gate position in per unit
$\overline{H}$	Per unit head at the turbine inlet
$\overline{P}_m$	Mechanical power in per unit
$\overline{q}_{nl}$	Water flow at no load in per unit
$\overline{q}_{fl}$	Water flow at full load in per unit
A_{TG}	Turbine gain $= \dfrac{1}{(g_2 - g_1)}$
g_1	Gate opening at no load
g_2	Gate opening at full load
D_p	Permanent droop
K_d	Temporary droop
T_d	Dash pot reset time
f_b	Base frequency of a system
f_b^+	Change in frequency in a system
${}^{MG}f_b$	Base frequency of a renewable micro-grid system
${}^{FD}f_b^+$	Change in frequency in the micro-grid system
P_b	Power in a system at base frequency
P_b^+	Change in power due to change in frequency
ΔP	Deviated power at the micro-grid system

D_c	Droop characterize coefficient
e_p	Power error
r_{cs}	Control signal
α	Firing angle
k_p, k_i	Proportional, integral gain for upper frequency threshold controller
v	Water velocity
R_e	Reynolds number
ρ	Water density
d	Pipe diameter for hydro storage unit
μ	Water viscosity
$\in$	Absolute roughness
f	Friction factor for steel pipe
l	Length of the pipe
H_L	Head loss
H_t	Total head to lift water
P_{gc}	Generation capacity of hydro storage unit
I	N Vector of source currents injected into each bus
V	N Vector of bus voltages
Y_{bus}	Bus admittance matrix
S_i	Net complex power injected into a bus

V_k, V_i	Voltages at bus k and i
Y_{ik}	Admittance between bus i and k
P_i, Q_i	Real and reactive power at bus i
P_{Ci}, Q_{Ci}	Calculated values of real and reactive power at bus i
P_{Gi}, P_{Di}	Real power generation and demand at bus i
Q_{Gi}, Q_{Di}	Reactive power generation and demand at bus i
$P_{sp,i}$	Specified real power at bus i
$\Delta P_i, \Delta Q_i$	Real and reactive power mismatches at any bus i
P_{TG}	Total real power generation
P_{TL}	Total real power demand
Q_{TG}	Total reactive power generation
Q_{TL}	Total reactive power demand
$P_{CG,i}$	Calculated value of real power generation at bus i
$P_{CD,i}$	Calculated value of real power demand at bus i
$Q_{CG,i}$	Calculated value of reactive power generation at bus i
$Q_{CG,i}$	Calculated value of reactive power demand at bus i
P_S	Real power output of the storage unit
Q_S	Reactive power output of the storage unit
J	Jacobian matrix

V_{abc_mg}	Three phase micro-grid voltages
$V_{\alpha\beta}$	Micro-grid voltage components in α-β reference frame
T_T	Transformation matrix
V_{DQ}	Micro-grid voltage components in d-q reference frame
T_r	Rotation matrix
P_c	Real power command to the inverter controller
Q_c	Reactive power command to the inverter controller
V_{Dc}, V_{Qc}	d-q voltage components of the power command
I_{Dc}, I_{Qc}	d-q current components of the power command
ϕ, θ	Phase angles of the micro-grid voltage and inverter output voltage

List of Abbreviations

CB	Circuit breaker
CERTS	Consortium for electric reliability technology solutions
CanWEA	Canadian Wind Energy Association
DGWS	Distributed generation with storage
DFIG	Doubly-fed induction generator
FC	Fuel cell
FESS	Flywheel Energy Storage
HGU	Hydro generation unit

MCFC	Molten carbonate fuel cell
NEDO	New energy and industrial technology development organization
NPEP	Newfoundland power energy plan
PV	Photovoltaic
PC	Power controller
PCC	Point of common coupling
PAFC	Phosphoric acid fuel cell
SSC	Storage system controller
SCR	Silicon controlled rectifier
SOFC	Solid oxide fuel cell
SS	Static Switch
WT	Wind turbine
WPGS	Wind power generation system
WESNet	Wind Energy Strategic Network
WPGS (n)	Number (n $\approx$ 0 to 9) of operational wind turbines in WPGS

Chapter 1

Introduction

1.0 Background

Wind energy is one of the fastest growing renewable energy that is utilized for commercial and domestic ratings around the globe. Technologies for wind power generation are rapidly expanding due to the high cost of energy derived from fossil fuel and nuclear fuel. Canada has a great potential for utilizing and integrating wind energy due to its longest coastline with wind resources. Canada is currently experiencing an annual 30% growth rate in wind energy development, which as of July 2007 has reached install capacity of 1588 MW. The Canadian Wind Energy Association's (CanWEA) goal is for 10,000 MW of installed wind energy capacity in Canada by the year 2010 which is sufficient to cater for 5% of Canada's electricity demand (www.canwea.ca). This wind energy can be a good celebrity forming the hybrid power system especially in the remote and isolated locations. Stand-alone hybrid power systems have gained popularity over the last few years. However, the power generated from the wind is not constant all the time as it behaves high degree of randomness. Hybrid system consisting of wind energy integration will be more beneficial if it's provided with storage system. The storage system could be long term or short term depending on the types of the hybrid power system. As the wind speed and the load of the isolated hybrid power system vary, introducing a of short term energy storage system, like flywheel storage can be a good solution to balance the load

and the supply. Flywheel storage can store energy from few seconds to a few minutes depending upon the size of the wheel.

Many years ago, pure mechanical flywheels were used solely to keep machines running smoothly from cycle to cycle, thereby render possible the industrial revolution. During that time several shapes and designs where implemented, but it took until the early 20th century before flywheel rotor shapes and rotational stress were thoroughly analyzed [1]. Later in the 1970s, flywheel energy storage was proposed as a primary objective for stationary power backup. At the same time, fiber composite rotors where built, and in the 1980s magnetic bearings started to appear. Thus the potential for using flywheels as electric energy storage has long been established by extensive research. More recent improvements in material, magnetic bearings and power electronics make flywheels a competitive choice for a number of energy storage applications [2]. The progress in power electronics, IGBTs and FETs, makes it possible to operate flywheel at high power ratings, with a power electronics unit comparable in size to the flywheel itself or smaller. The use of composite materials enables high rotational velocity with power density greater than that of chemical batteries. Magnetic bearings offer very low friction enabling low internal losses during long-term storage. High speed is desirable since the energy stored is proportional to the square of the speed, but only linearly proportional to the mass.

The energy scenario in the world is calling for efforts towards more efficient use of electrical energy, as well as improved quality of its delivery [3], [4], and [5]. Due to limited budgets, the alternative may result in different levels of supply quality. This issue involves the usage of equipments applying the concept of energy storage devices

like batteries or flywheels. The demand for this equipment is increasing and thus their usage. The type of energy storage system that is most widely researched and used especially in the last period, is the Flywheel Energy Storage System (FESS). Due to the advancements in machines and power electronics, the flywheel is becoming more popular. Many feasible projects employing the FESS have been implemented all over the world.

The Flywheel Energy Storage System can have many applications including uninterruptible power supplies (UPS), dynamic voltage compensators, overload compensators, and start-up of standby diesel generators [6], [7]. In the overload compensation, the FESS supports the main grid by supplying power to part of the load. This occurs when there is a voltage or frequency dip in the main grid and thus it is not capable, for a few seconds, to supply all the power needed by the load. Therefore, the main purpose of the flywheel is to accumulate rotational kinetic energy which can be injected into the electric system whenever it is required.

Flywheels are complex constructions where energy is stored mechanically and transferred to and from the flywheel by an electrical machine. The electrical machine should work as a motor to transfer electrical energy to the flywheel and as a generator to convert the energy stored into the flywheel [7], [8], [9]. When acting as a motor, the electric energy supplied to the stator winding is converted into mechanical energy, increasing the speed of the flywheel. In generator mode, kinetic energy stored in the rotor is converted into electrical energy. The motor/generator part has a large upgrade

potential and its design is continuously improving. Figure 1.1 shows the basic layout
of a flywheel energy storage system.
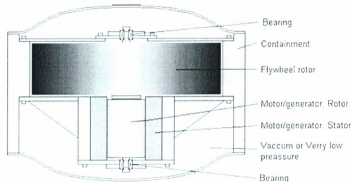
Figure 1.1 Basic layout of a flywheel energy storage system.

In theory, it would be advantageous to build a generator that produces high voltage
and low current, which would result in high power supply and low power losses. The
fast rotation of flywheel rotors is suitable for direct generation of high voltage.

The flywheel energy storage system (FESS) is basically composed of an electric
machine (either AC or DC) and its controlling power electronics [10]. Therefore there
are a lot of advantages for the FESS such as its high power efficiency, mechanical
load coupling, and using no hazardous chemicals; thus being environment friendly.
The efficiency of the whole system is directly proportional to the efficiency of the
power electronics and machine used. A regular machine nowadays has efficiency
above 85%, while the efficiency of the power electronics nowadays exceeds 95%.

Many projects based on the flywheel storage have been implemented in several countries, especially USA and several European countries. However, with the advancements in power electronics, machines, materials and magnetic bearings of machines, new ideas are being researched and new projects are implemented. High speed flywheel systems (more than 30,000 rpm) are now in the prototype stage and it is expected that these systems will be in market, within the coming 10 years. Although, the flywheel as an energy storage system has been used from thousands of years, research in this subject is still active and it is expected to keep in progress for years to come. A survey of relevant literature shows that the maximum speed reached in experiments is around 60000, which is suffering from error generated by mechanical vibrations.

There are a number of attributes that make flywheels useful for applications, where other storing units are now being used due to the following advantages:

- High energy density.
- Minimum capacity degradation, the lifetime of the flywheel is almost independent of the depth of the discharge and discharge cycles. Also it can operate equally well on shallow and on deep discharges.
- Minor periodic maintenance.
- Short recharge time.
- Scalable technology and universal localization.
- Environmental friendly materials.

1.2 Types of Energy Storage System

Energy storage systems can be divided into short and long-term response, depending on their application [71]. Technologies with high power density and with the ability to respond to requests in short time, like flywheels, capacitors or superconducting magnetic coils, belong to the so-called short-term response energy storage devices category. Energy storage devices with the capability to absorb and supply electrical energy for long periods of time like pumping hydro, batteries, and compressed air and hydrogen fuel cells, are considered the long-term response category. Power systems are experiencing significant changes in operational requirements that result from the sector restructure and evolution. Largely interconnected network and distributed, renewable generation lead to more complex and less secure power system operation. Energy storage appears to be beneficial to utilities since it can decouple the instantaneous balancing between the demand and the supply. Therefore, it allows the increased asset utilization, facilitates the penetration of renewable sources and improves the flexibility, reliability and efficiency of the grid. However, the use of energy storage devices has not expanded significantly because of the state of technological developments and the price of energy storage devices. Nonetheless, there are several high performance storage technologies available today, or at an advanced state of development, which enables a new range of potential applications. For example, the issues related to the increasing integration of renewable sources in power systems have been one of the main drivers for these developments. Long-term response energy storage devices for power systems applications can usually absorb and supply electrical energy during minutes or hours and can contribute to the energy

management, frequency regulation and grid congestion. On the other hand, short-term response energy storage devices are usually applied to improve power quality, particularly to maintain the voltage stability in power systems, throughout contributions during transients (few seconds or few minutes).

1.3 Long-Term Response Energy Storage Devices

There are different long-term response energy storage technologies are already available today. A brief description of these devices is presented in the following paragraphs [71].

i. *Pumping hydro storage system*:

In pumping hydro storage system, a mass of water at a relatively high elevation represents a potential or stored energy. During peak hours the water in the upper reservoir is lead through a pipe downhill into a hydroelectric generator and stored in the lower reservoir. During off-peak periods, the water is pumped back up to recharge the upper reservoir and the power plant acts like a load in power system.

ii. *Batteries*

Batteries store energy in electrochemical form creating electrically charged ions. When the battery charges, a direct current is converted in chemical energy, when discharges, the chemical energy is converted back into a flow of electrons in direct current form. There are two main types of batteries, which are:

1) Electrochemical

Electrochemical batteries use electrodes both as part of the electron transfer process and store the products or reactants via electrode solid-state reactions.

2) Redox Flow

Redox flow batteries are storage devices that convert electrical energy into chemical potential energy by charging two liquid electrolyte solutions and subsequently releasing the stored energy on discharge.

iii. *Compressed Air*

In compressed air energy storage, power during off-peak hours is taken from the grid and used to pump and compress air into a sealed underground cavern to a high pressure. The compressed air is mixed with natural gas and burnt together, in a conventional gas turbine. This method is actually more efficient as the compressed air will lose less energy.

iv. *Hydrogen Fuel Cell*

During the operation of a fuel cell, hydrogen is ionized into protons and electrons, and the hydrogen ions are transported through the electrolyte to the cathode by an external circuit (load). At the cathode, oxygen combines with the hydrogen ions and electrons to produce water. The hydrogen fuel cell system can be reversible, allowing electric power consumption for the production of hydrogen and that can be stored for later use in the fuel cell.

1.4 Short-Term Response Energy Storage Systems

Short-term response energy storage systems are used to aid power systems during the transient period after a system disturbance. The main short-term energy storage devices and their operation are classified as: [71].

A. *Flywheels*

Flywheels store kinetic energy in a rotating mass. Such equipments have typically been used as short-term energy storage devices for propulsion applications such as powering train engines and road vehicles, and in centrifuges. In these applications, the flywheel smoothes the power load during deceleration by dynamic braking action and then provides a boost during acceleration.

B. *Super Capacitors*

Super capacitors are electrochemical double layer capacitors that store energy as electric charge between two plates, metal or conductive, separated by a dielectric, when a voltage difference is applied across the plates.

C. *Magnetic Superconducting*

Superconducting magnetic energy storage (SMES) systems convert the ac current from a power system into the dc current flowing in the superconducting coil and store the energy in the form of a magnetic field. The stored energy can be released to the ac system when required.

Table 1 flywheel battery comparison with lead-acid and Superconducting battery types

Table 1.1

	Lead-acid battery	Flywheel battery	SMES
Storage mechanism	Chemical	Mechanical	Electrical
Life (years in service)	3–5	>20	~20
Technology	Proven	Promising	Promising
Number of manufacturers	~700	~10	~1
Annual sales (in US $millions)	~7000	~2	A few
Temperature range	Limited	Less limited	Controlled
Environmental concerns	Disposal issues	Slight	Slight
Relative size (equivalent power/energy)	Larger	Smallest	In between
Practical time to hold a charge	Years	Hours	Days
Price, per kilowatt	$50–$100	$400–$800	>$300

SMES = Superconducting magnetic energy storage.   Source: University of Texas

Table 1 represents the comparison among the three energy storage system such as Lead –acid battery, superconducting magnetic storage and flywheel storage system. From the above table we see that the flywheel is a mechanical battery with life time more than 20 years. It is also superior to the other two types in regards to temperature range, environmental impact and relative size.

considering the energy storage system for   an isolated wind diesel hybrid power system to mitigate the voltage sag due to sudden load variation , the flywheel energy storage system appears to be the most appropriate and efficient. The average and peak load of Ramea Island is 270KW and 1200KW respectively. Newfoundland hydro is going to introduce another three 100KW new wind turbines with the hydrogen fuel cell storage system. The hydrogen fuel cell consists of three units as follows:

➤ Electrolyzer (efficiency is about 70%)

➤ Hydrogen Storage (efficiency is about 80%)

➤ Hydrogen Generator (efficiency is about 45%)

The overall efficiency is very low (about 25%) with respect to pumped hydro storage system (efficiency is about 75%) and flywheel energy storage system (efficiency is about 90%).
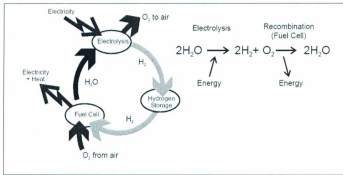
Fig. 1.2 Hydrogen fuel cells System (The hydrogen cycle)

Wind turbine can generate electric power, which may vary due to wind speed changes. For operational conditions, hydrogen storage is not sufficient as short term energy storage. However flywheel energy storage system can be a better choice to balance the sudden peak load and act as a short term storage system. Moreover, the average load of Ramea is less than 300 kW; it requires operating at least one diesel generator.

The following section presents the different applications of flywheel energy storage systems:

Peak power buffers – The flywheel could be used in an electric vehicle to eliminate peak currents that prolongs the battery life.

Wind-diesel generator with a flywheel energy storage system – The goal of this system was a unit where the regular wind oscillations were compensated by the flywheel, supplying active and reactive power to compensate both frequency and voltage of the network.

Flywheel for photovoltaic system – Despite the many benefits of using solar energy, its frequent unavailability makes it inappropriate for many applications. Consequently it is often necessary for photovoltaic (PV) systems to have an energy storage capability such that the excess energy output of the PV cells can be used at a time when solar energy is unavailable. As an example of this kind of application, in a photovoltaic equipped building situated in Hong Kong, the load supply time was prolonged from 9 a.m. - 3 p.m. to 8 a.m. - 6 p.m., by adding a flywheel.

Harmonics – The basic principle of flywheel harmonic compensators is similar to the active filter using an inverter. However the flywheel system has an additional energy storage capability. In the active filters, compensating currents are estimated for reducing the harmonics by calculating harmonics of the load current. Then the estimated current is generated by an inverter.

Flywheel in distribution network – The flywheel can be used to maintain high quality electric power and guarantee a reliable power supply from the distribution network (it is able to keep the voltage in the distribution network within 98–102% and with the ability to supply 10 kW of power for 15 min).

High power UPS system – For a high power system, 25 flywheels are connected 25 in parallel, with possible applications on energy supply for plasma experiments, accelerations of heavy masses (aircraft catapults on aircraft carriers, pre-acceleration of spacecraft) and large UPS systems. Similar permanent magnets flywheels have previously been tested in urban traffic buses and rail systems with a resulting energy save of up to 40%.

UPS system – As an example of this kind of application, four flywheels based dynamic UPS systems are connected to the distribution network; it results in a significant improvement in power quality. A transformer was required between the flywheel storage system and the medium voltage network.

Aerospace applications – A flywheel storage unit is intended to replace a battery storage unit onboard the International Space Station, a comparison between the flywheel and the NiH2 battery has shown that a flywheel system is 35% lighter and 55% smaller in volume.

1.4 Literature Review

1.4.1 Papers Review

Silva Neto and Rolim, G. in [19] presents a flywheel energy storage system (FESS) using a switched reluctance machine (SRM). This system is to be used as a static shunt compensator. Superconducting magnetic bearing is used to decrease the friction

losses. SRM provides a wide range of operation from zero up to several ten thousands rpm in addition to its having high reliability.

The figure below shows the circuit implemented in the FESS:
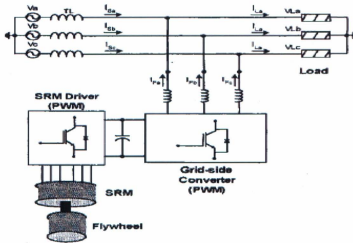
Fig. 1.3 Control of power electronics circuit for flywheel energy

The acceleration of the SRM is controlled by measuring the difference between the dc link capacitor voltage and a given reference value (as shown below):
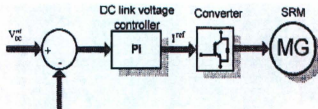
Fig. 1.4 PI Controllers for a switched reluctance machine

Increasing speed rather than mass:

From experimental results, it was shown that the energy of the flywheel can be increased better by increasing the speed while keeping the mass constant rather than increasing the mass and keeping the speed constant. However, some problems arise with increasing speed. These are:

- Increased losses due to air resistance
- Increased probability of mechanical failure due to higher speed
- Increased losses due to bearing friction
- Increased magnetic losses due to higher frequency of stator currents.

Magnetic losses can be reduced by correctly designing the machine with proper selection of the core material. Windage and friction losses can be reduced by using vacuum and superconducting magnetic bearing. As a conclusion, this paper has presented the SRM flywheel system and showed that SRM is a good choice as a driving machine, and thus the power quality in electric energy systems has been enhanced. In [20], Jeoung, H. and Choi, J. has describe a flywheel energy storage (FESS) using high temperature (HTS) superconductive magnetic bearing and permanent magnet synchronous motor. Different types of motor/generators have been examined. An induction motor is robust, inexpensive, and the motoring and regenerating power can be controlled by adjusting the slip power. However, it is difficult to have high efficiency at high speed operation. Also, other types like reluctance motors and synchronous motors have been studied, but each has its problems when considering HTS magnetic flywheel system. It is proved that the validity of this system used (HTS magnetic Flywheel system) is superior to the conventional electro-mechanical flywheel system. The maximum speed reached in the experiments is 40,000rpm.

Johnson, B, Law, J, Hess, J and Samineni, S. in [21] have shown the Modeling and Analysis of a Flywheel Energy Storage System for Voltage Sag Correction. Flywheel systems operating at low speeds have some advantages like: lower cost and use of proven technologies. Disadvantages are less stored energy per volume and higher losses. This paper examines a low speed flywheel system coupled to an induction motor. In this circuit, two rectifier/inverters are used. It was shown that the main advantage of the FESS tested is its low cost, high energy density, and the efficiency in mitigating long duration voltage sags. Advanced Motor Control Test Facility for NASA GRC Flywheel Energy Storage System Technology Development Unit in [22] discussed the operation and control of a flywheel mounted on a 4-pole permanent magnet synchronous machine. This synchronous machine needs control due to its sensitivity to speed changes. The control method is using the d-q axes control method. The motor is controlled successfully at a speed of 20000 rpm. Testing speeds reached 60000 rpm but the control method was unable to eliminate the high value of speed oscillation which caused in turn a large error in the current supply. Kenny B, Kascak P and Mackin M in [23] describes world's major problem is in energy storage rather than energy production. Flywheel provides simple, short term energy storage. The limitations of battery technology hindered the widespread use of many electric vehicles and motivated the use of new-old electric storage system. Flywheels can be used for many electrical applications and in combination with other generator systems to cover short-term power fluctuations. Also they can be introduced to the telecoms market to provide secure, autonomous power supply for network nodes.

Flywheels can be easily integrated to electric machines due to their rotational characteristics. The design approach consists of strong light weight materials and solid-state electronics. The important design aspect of the flywheel system is that the kinetic energy of a rotating body is directly proportional to the moment of inertia and the square of the angular velocity, so we seek for a massive, high-speed flywheel. The flywheel should be rigid and balanced and is usually made from carbon and glass fiber composite material. A cylindrical shaped flywheel has many advantages in terms of maximum energy, avoiding resonance, and space allocation.

The most important operational aspect is to maintain a constant voltage to the load; i.e. to compensate any power supply failure or frequency variations. At start-up, the flywheel will rotate gaining kinetic energy till it reaches its maximum speed. At this moment, it will be switched off allowing for energy dissipation until zero due to frictional losses. Then the set will be turned on again till reaching the maximum speed again. The maximum speed of the flywheel is determined by the construction. The stored kinetic energy will be supplied to the load when needed. Note that not all stored energy is recoverable.

The power flow into and out of the flywheel should be controlled. Thus its speed is controlled to supply constant frequency and supply. This is done by means of a three phase voltage source inverter that operates as an inverter when power is supplied to the flywheel and as a rectifier when power is drawn from the flywheel. Benefits can be summarized as: wide operating temperature range, high cycling capability, guaranteed energy content, long design life, maintenance free, and low losses. In [24], a doubly fed variable speed wind induction generator connected to the grid associated to a flywheel energy storage system (FESS) is investigated. The dynamic behavior of a

wind generator, including the models of the wind turbine (aerodynamic), the doubly fed induction generator (DFIG), a ac/ac direct converter, the converter control (algorithm of VENTURINI) and the power control of this system, is studied. Also investigated is a control method of the FESS system, which consists of the classical squirrel-cage induction machine, supplied off the variable speed wind generator (VSWG) through a rectifier–inverter cascade arrangement. Simulation results obtained on the basis of the dynamic models of the wind generator are presented, for different operating points, to demonstrate the performance of the proposed system.
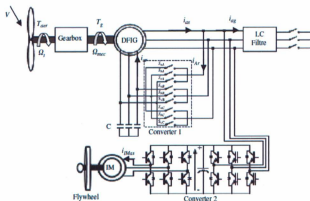
Fig. 1.5 (a) Schematic of the studied device topology.
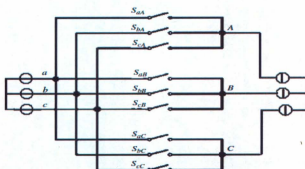
Fig. 1.5 (b) Matrix converter topology.

The control of flywheel battery is researched in [25] by K. Ghedamsi, D. Aouzellag and E.M. Berkouk. The motor/generator is three-phase permanent magnet synchronous motor. Vector control is used to control flywheel battery charge and Electrode Plate Control is embedded in vector control. Through controlling the duty cycle of IGBT, the flywheel battery discharges with steady voltage. The experimental result has verified that this method was effective in flywheel battery storing energy and releasing energy process. Flywheel battery is now considered as enabling technology for many applications, including space systems, pulse power transfer for hybrid electric vehicles and Uninterruptible Power Supplies (UPS), telecommunications are some others alternative techniques for energy storage have been proposed, example for lead- acid batteries, superconductor, compressing air and capacitors. In comparison with others, the flywheel battery is a kind of clean energy storage system and has lots of advantages. It has high efficiency, high energy density, long serve life and no environmental pollution. It can improve the quality and reliability of the power network. In this study, a kind of new control method, Electrode Plate Control (EPC), is introduced to control the flywheel battery charge and discharge processes. EPC is a kind of nonlinear control method, based on the physical model that a charge is between a pair of electrode plates.

The flywheel battery is an electro-mechanical approach to energy storage. To store electricity, a motor is used to convert the electricity from an external source into the rotational energy of a flywheel. Using the motor as a generator, then extracting energy retrieves the stored energy. In general, a complete system of flywheel battery consists of four parts (1) the flywheel that stores energy, (2) bearings that supports the flywheel, (3) a motor/generator and (4) power electronics and control electronics.

The amount of energy stored and released, E is calculated by means of the equation:

$$E = \frac{1}{2}I(\omega_h^2 - \omega_l^2)$$ .... (1.1)

Where:

I = The moment of inertia of the flywheel.

ω_h = High operating speed.

ω_l = Low operating speed.

As shows in Fig. 1, the experiment flywheel battery system in this study consists of a digital controller, a three-phase rectifier, a intelligent inverter, a flywheel, a three-phase PMSM, a PC. The digital controller consists of a DSP control board based on TMS320LF2407 and interface board.
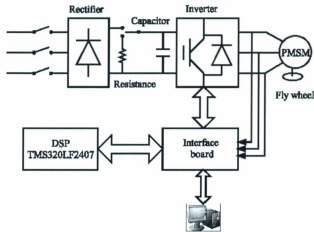
Fig. 1.6 Flywheel Battery System

Electrode Plate Control (EPC): If a positive charge is between a pair of positive electrode plates, under the electric power, the charge will stay at the balance position. If the positive charge represents the control object, then electrode plates control model can be constructed in phase plane, as shows in Fig. 2.

Fig. 1.7 Model of PEC

+U0 and -U0 are the control power to the control object. L1 and L2 are the distance between point A and the plates. When the control object is at position A, the control effect of +U0 is strengther than of -U0, because of the distribution of the field. So the control power UA is positive and the control object move to the balance position of the electric field. When the control object is at position B, the condition is reverse.
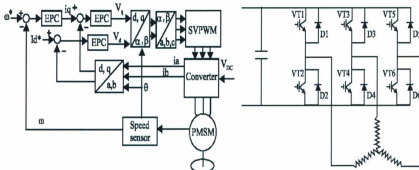
Fig. 1.8 (a) Vector Control of PMSM   (b) Three Phase Inverter Bridge and Windings of PMSM

The vector control of PMSM is used in flywheel battery charge process, the controller in vector control is EPC. The control system is shown in figure 3. The boost chopper principles are used in the flywheel battery's discharge process. According to the counter electromotive force of PMSM the IGBT is open and closed. Every IGBT is works in 600 electrical angles.

Based on mathematical model of PMSM, EPC controller is used to control charge and discharge process. The power change of flywheel battery for energy storage is shown in Fin. 7.In the energy storage process the power increased rapidly. This confirmed the advantage that flywheel battery can store energy at high power. The voltage change in energy release process shows in Fig. 8. The voltage maintained 120 V in 2.8 sec, and then declined sharply. The flywheel battery can output stable voltage for a certain period of time. The results of the experiment verified that the energy storage and release processes of flywheel battery can be can be effectively controlled by EPC controller.
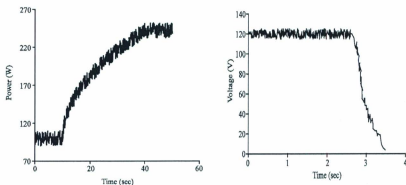
Fig. 1.9 (a) Power Change of Flywheel Battery for energy Storage   (b)

Voltage Change of Flywheel Battery in Energy Release

Losses and Efficiency of a Flywheel Energy Storage System with Permanent-Magnet Synchronous Machine Associated to a Variable-Speed Wind Generator have been presented by Guo Zhenyu, Mu Xiaoping and Bai Zhifeng in [26]. The flywheel energy storage systems (FESS5) are suitable for improving the quality of the electric power delivered by the wind generators and to help these generators to contribute to the ancillary services. This paper investigates the energetic performances of a low-speed FESS with a Permanent Magnet Synchronous Machine (PMSM) in view of its associated to a wind generator. In the last years, Flywheel Energy Storage Systems (FESS5) has been rediscovered by the industrials due to their advantages in comparison with other energy storage systems. FESSs have thus found a specific application for the electric power quality, as far as the voltage and frequency maintenance between imposed limits is concerned. By virtue of their high dynamics, long lifetime and good efficiency, FESSs are well suited for short-term storage systems, which are generally sufficient to improve the electric power quality. In the case of variable-speed wind generators (VSWGs), by using the power electronics, energy generation and storage systems can be coupled via a DC bus. In such a configuration, the FESS ensures the DC-bus voltage control, thus contributing to the generation/consumption balance. The power converter connected to the network can then be concerned with the mains voltage and frequency control, and the wind generator can contribute to the ancillary services. For accomplishing these objectives, a generating system, which must be able to feed isolated loads or to be integrated in the network, is here considered. The wind generator must then work without auxiliary source to contribute to the generation! Consumption balance, and to set the adequate frequency and voltage. A FESS is linked to the DC bus. The connection to the network

is achieved through a LC filter and a transformer. The LC filter ensures a good voltage quality, and is well suited for feeding isolated loads. The reference value of the power generated to the network is determined by means of a fuzzy-logic supervisor and the voltage and frequency control is achieved using a resonant controller In general, the flywheel for a FESS associated to a VSWG is built from steel, and has a maximum rotational speed of 10,000 rpm [1]. Hence, FESSs do not require to design a special electric machine instead of a classical one. Moreover, no magnetic bearings and vacuum are necessary.

In this study, a low-speed FESS with a permanent magnet synchronous machine (PMSM) is considered. FESS is connected to the DC bus of the system in order to control the power flow from the VSWG to the network. Fig. 1 presents the VSWG-FESS assembly under study.
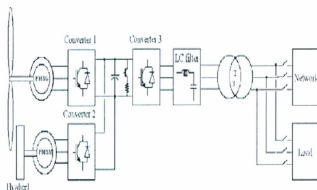
Fig. 1.10 Diagram of the VSWG-FESS assembly under study

This test bench of 3 kW enables the performance analysis of the VSWG connected to the AC grid or to an isolated load. The wind turbine is emulated by a DC machine. The test bench has a modular structure, allowing different topologies of the VSWG-FESS assembly.

Dynamic performance analysis of a FESS with PMSM associated to a VSWG has been presented in the paper. Simulation and experimental results, for the FESS losses and efficiency on a 3 kW test bench have been given and comparatively assessed. In [27] a new series power-conditioning system using a matrix converter with flywheel energy storage is proposed to cope with voltage sag problem. Previous studies have highlighted the importance of providing adequate energy storage in order to compensate for deep voltage sags of long duration in weak systems. With the choice of flywheel as a preferred energy storage device, the proposed solution utilizes a single ac/ac power converter for the grid interface as opposed to a more conventional ac/dc/ac converter, leading to higher power density and increased system reliability. This paper develops the dynamic model for the complete system, including the matrix converter in dual synchronous reference frames coupled to the flywheel machine and the grid, respectively. The dynamic model is used to design a vector control system that seamlessly integrates functions of compensating load voltage and managing energy storage during voltage sag and idling modes. The numerical simulation and experimental results from a laboratory-scale hardware prototype are presented to verify system performance. As the reliability and availability of the power system continue to improve, power interruptions have become rare events in power distribution systems. However, voltage sags arising from faults on parallel feeders are

still a major power quality concern in terms of the severity of the incurred economic losses to sensitive loads. Due to the typical radial structure, the distribution system is inherently vulnerable to weather conditions, falling tree branches or animal contacts, and insulation failures or human activity. At the distribution level, the voltage sags occur when a short circuit fault takes place on a parallel feeder. In addition, the sag depth depends on the distance from the fault location and impedance profile of the system. While power interruptions do occur when the protection devices operate on the faulted branch, they do so at a smaller frequency compared with the occurrence of voltage sags (number of parallel branches versus the faulted branch).To cope with the voltage sag problem, a series compensation device, commonly called dynamic voltage restorer (DVR), has been applied as a definitive solution due to the advantages of the series compensation over the shunt compensation in terms of the required power rating for typical voltage stiff systems. The first DVR was introduced in 1994 as a result of collaborative effort between Westinghouse (presently Siemens), EPRI, and Duke Power . Among the existing DVR topologies, various different types of switching power converters have been employed.
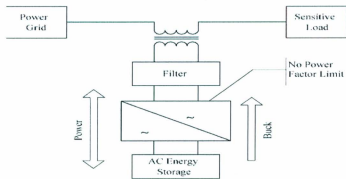
Fig1.11 (a) System-level requirements for DVR
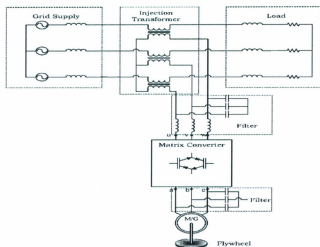
Fig1.11 (b) Proposed architecture of the DVR system converter topology.

This paper has presented a DVR system employing matrix converter and flywheel energy storage. The overall proposed system is modeled in two reference frames that are synchronized with the grid and the machine back EMF, respectively. The resulting system model is challenging for controller design due to the time-varying modulation and nonlinearity caused by the matrix converter coupling. To overcome the control design challenge, a nonlinear input decoupling strategy is put forth, which allows the application of classical servo-control design methodology to the reduced-order subsystem, namely, the grid interface LC filter. The nonlinear time-varying input decoupling approach may be employed as very useful methodology in dealing with power conversion systems with ac/ac power converters.

From the above literature review it is seen that flywheel energy storage system is the most promising energy storage system now a days because of its high power storing

capacity. The life time of flywheel is much higher than any other storage system. Flywheel can be used to mitigate the voltage fluctuation, frequency regulation, supplying clean energy at high density.

A flywheel energy storage system is consisting of a motor/generator set along with the flywheel. Motor is used for charging mode taking power from the grid. Generator is used for the discharge of the flywheel and flywheel's kinetic energy is converted into electrical power for a short period of time. For the bidirectional power flow there must be some power electronic drive circuits such as converter, inverter, chopper, rectifier etc. There also must some controller to control the power flow to and from the flywheel. The controller can be a PID type controller, Fuzzy logic based controller or any peripheral interface controller. Dynamic voltage restorer can be used for the voltage sag mitigation. Electrode Plate Control (EPC) can be used for controlling the charge and discharge of the flywheel battery. G. Zanei and E. Cavenini in [29] talk about the application of flywheel as an uninterruptible power supply (UPS) and a dynamic voltage compensator. The figure below shows the circuit used: The experiment done uses an AC machine coupled to a flywheel. There are three modes for the system and each includes a set of switches closed and others open: *The charging mode*: in which the grid supplies power to the load and to the machine acting as a motor resulting in the rotation of the flywheel. Rect/Inv1 in this case acts as a rectifier to change from AC voltage from the supply to DC voltage and then Rect/Inverter acts as an inverter to change the DC voltage again to AC to feed the machine.*Compensation mode*: in which the flywheel supplies a percentage of the load and thus supplements the supply in feeding the load. In this case the machine acts as a generator, Rect/Inv 1 acts as a rectifier and Rect/Inv 2 acts as an inverter.

☐ *UPS mode*: in which the flywheel supplies the entire load and the grid is disconnected from the load. Rect/Inv 1, Rect/Inv 2 and the machine are as in the compensation mode.

The inverters are controlled by PWM signals. What is interesting in this paper is the use of series transformers needed in the case of UPS mode to provide a wide range of operation of the system. If the voltage dip that occurs at the load is 40V, then the flywheel connected to the generator of rating 277 V rms (this is the rating used) need to be converted to 40V by using very small modulation index of SPWM firing signals.
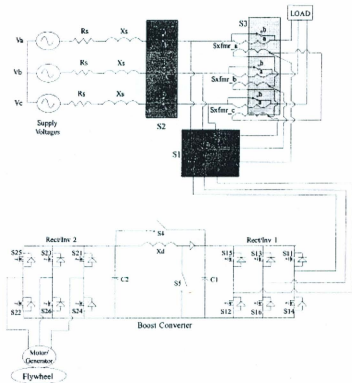
Fig. 1.12 Flywheel Energy Storage Systems

This is undesirable as we must use in this case high frequency high amplitude pulses. To overcome this problem, the transformer ratio is 5:1. In this case, 40V dip at the load will require 200V from generator which increases modulation index.

In case the voltage dip is 100V, we must inject 500V by the generator. Here, the boost converter is used which can raise the voltage of the generator and thus supply the voltage needed by the load. Thus a novel control scheme is used in this experiment and the result is an FESS which acts as a UPS or dynamic voltage compensator and allows for a sufficient range of operation.

Michael Mathew in [30] clearly depicts the importance of the flywheel geometry design selection and its contribution in the energy storage performance. This contribution is demonstrated on example cross-sections using computer aided analysis and optimization procedure. Overall, the problem objective is formulated in terms of Specific Energy value and its maximization through the selection of the best geometry among the predetermined five cross-sections. Using the available technology at hand, we could very well make fast but crucial improvements in the advanced research areas requiring flywheel utilization, where engineers are frequently confronted with the limitations on magnetic bearing load carrying capacity, size limitations and efficiency.

In [31] the research on voltage sag and its mitigation techniques have received a lot of attention. Most of the sag mitigation studies concentrated on storing energy in capacitors or batteries. In this paper a flywheel is used to store energy which can be injected back into the power system during sag period. A shunt voltage compensation scheme consists of power electronic interface, coupling transformer and an energy storage unit are the structure of the system. In this case, the flywheel is coupled to a dc machine which is used for energy conversion purpose. The stored energy is used for

30

sag compensation during the starting of a large induction motor load. Simulation and experimental works have been performed and a good agreement has been obtained.

Bjorn Bolund, Hans Bernhoff and Mats Leijon [32] in their article, a 200kW permanent magnet air gap winding motor/generator with axial flux were simulated. This motor/generator setup incorporates high voltage technology with the use of permanent magnets and an air wound stator. The simulation topology used was partly chosen for simulation simplicity and can most likely be enhanced. The simulated motor/generator is intended for a flywheel storage system situated in e.g. a bus. However, this flywheel technology is scalable and larger machines can be constructed for the applications of stabilizing the electric grid.

In [33] based on the progress of heavy-load HTS bearings the technical concept and recent development results of a new high- efficient compact 5 kWh/250 kW FESS for uninterruptible power system (UPS) and power quality function is reported. In a first step they have been designed, constructed and tested a new compact HTS magnetic bearing capable to stabilize a 400 kg flywheel rotor safely. At 78.5 K the maximum axial load of the cylindrical 200 mm HTS bearing was 8000 N at initial stiffnesses of 3 kN /mm and 1.5 kN /mm for axial and radial forces, respectively.

In [34], it presents an experimental characterization of a flywheel energy storage system. The device is based on steel seamless tube mounted as a vertical axis flywheel storing kinetic energy. The motor/generator is a Permanent Magnet Synchronous Machine controlled by an AC-AC Matrix Converter. The matrix control method uses a

discrete-time model of the converter system to predict the future values of the input currents for all the 27 possible output voltage vectors generated by the matrix converter. An optimal controller minimizes current errors using a weighted cost functional. This flywheel and control process is intended for dynamic voltage restorer (DVR) to mitigate voltage sags.

A flywheel cell intended for multi-flywheel cell based energy storage system is proposed in [35]. The flywheel can operate at very high speed in magnetic levitation under the supports of the integrated active magnetic bearing and a passive magnetic bearing set. 3D finite element analyses were applied to verify various configurations of passive magnetic bearing. The feasibility of PID controllers for the flywheel cell was evaluated by simulation study.

1.5 Objective of this Thesis

The main objective of this thesis is to design and develop a short term energy storage system for the isolated grid wind-diesel hybrid system of Ramea Island of Newfoundland, Canada.

The main steps for developing such a system are:

i)   System sizing based on the minute ac load variation data and wind speed data of the isolated grid.

ii) Steady state simulation in HOMER software to find out economical aspects of the hybrid power system.

iii) Dynamic Modeling and Simulation of Ramea Hybrid System in Simulink to observe the system dynamics.

iv)   Experimental Setup, test results and design of Control system for verification and implementation of the Flywheel Energy Storage System.

1.6 Organization of the Thesis

This thesis consists of five chapters. In the first chapter, introduction, literature reviews and objective of this research have been described. Chapter 2 comprises system sizing and steady state simulation of the wind-diesel-hydrogen hybrid power system of Ramea with flywheel energy storage system. System sizing is one of the most important parts of this chapter. System economics and steady state behavior are also discussed in this chapter. In chapter 3, dynamic modeling and simulation of Ramea hybrid power system has been done. Chapter 4 is comprised of the experimental setup and test result of a flywheel energy storage system. Detail control strategy, parameters and different instrumentations are described in this chapter. Chapter 5 is the conclusion and recommendation for future work.

Page 34
Missing from
Original Book

Page 35
Missing from
Original Book

Page 36
Missing from
Original Book

Chapter 2

System Sizing and Simulation of Flywheel Energy Storage System

2.1 Overview of the System:

Ramea is a small island 10 km from the south coast of Newfoundland. Population is about 700 and their occupations are traditional fishery. The latitude and longitude of this remote island are 47.519525' and 57.4011889°. The scenic community has all the amenities required for a small town. Fresh water is supplied from Northwest Pond and is treated in a newly constructed water treatment plant. A Newfoundland & Labrador Hydro power plant provides electricity for the community. Ramea power system comprised of three diesel generators, six squirrel cage induction generator based wind turbines, and three permanent magnet synchronous generators based wind turbines, an electrolyzer, three hydrogen storage tanks, five hydrogen generators, and time varying loads. In this chapter, a flywheel energy storage (FESS) system is proposed and added to Ramea hybrid system. The sizing of the proposed FESS is carried out using Homer software.
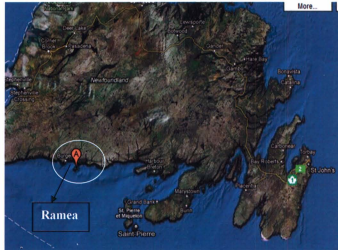
Figure 2.1: Location of Ramea Island
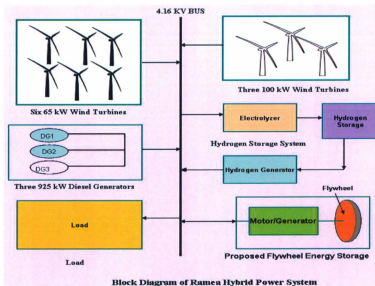
Figure 2.2: Ramea hybrid power system block diagram with the proposed
Flywheel Energy Storage System (FESS).

2.2 System Sizing using HOMER Software

Sizing a flywheel energy storage system critical for balancing the load and the supply. Maximum ramp up of load within a short period of time must be taken into account when sizing a flywheel energy storage system. Dimensions, materials of the wheel, maximum rotational speeds, etc are also required for calculating an optimum size of FESS. Some software can help to calculate the optimum size of FESS according to the nature of load data and source data. The 'HOMER' modeling software is used to calculate the optimum size of the proposed flywheel energy storage system. HOMER software is a modeling tool which is used to size stand-alone or grid-connected power system, as well as to analyze system economics and electrical properties. The HOMER energy modeling software is a powerful tool for designing and analyzing hybrid power systems, which contain a mix of conventional generators, cogeneration, wind turbines, solar photovoltaics, hydropower, batteries, fuel cells, hydropower, flywheels and biomass. For stand-alone or grid connected system, HOMER software helps to determine the optimal utilization of distributed generation units in hybrid power system. Also HOMER software can determine the economic feasibility of a hybrid energy system and optimize its design which allowing users to understand its operation. As distributed generation and renewable power projects continue to be the fastest growing segment of the energy industry, HOMER software can serve utilities, telecoms, systems integrators, and many other types of project developers - to mitigate the financial risk of their hybrid power projects.

From the system sizing it is found that at least one 25 kWh rated capacity FESS is necessary for Ramea hybrid power system. Smart energy (SE25) FESS from Beacon

Power Corporation is used for the system sizing which has highly cyclic capability, smart grid attributes, 20-years design life and sustainable technology.

2.3 Components Detail of Ramea Hybrid Power System:

Ramea power system comprised two types of wind turbines- Windmetic type (65kW of each) and North Wind (100kW) type. The diesel generators are rated at 925 kW each, Electrolyzers is rated at 200kW and Hydrogen generators are rated at 250 kW. The ratings and the number of operating components have already been decided by Newfoundland Hydro. Hence the capital cost, replacement cost, operation and maintenance (O&M) cost and operation period have to be assigned. The system has two feeder AC buses at 4.16 kV. The following section describes each of the component details, components parameters ascription, resource availability and optimized results.

2.3.1 Windmatic Wind Turbines (65kW)

Six WM15S rated at 65 kW have been selected for this site. The capital cost, replacement cost and O&M cost are as $ 90,000, $ 70,000, and $ 1200 per year respectively for each unit. All these cost information have been obtained from NL Hydro [36]. Each 65 kW AC wind turbine has a hub height of 25 m and an operation life time of 20 years. This information is also found from [37]. From the power curve of wind turbine in Figure 2.3, it can be seen that the cut-in, rated and cut-out wind speeds are 4 m/s, 15 m/s, and 23 m/s respectively. It is worth mentioning that the capital cost includes the shipping and installation cost of $ 30, 000 for each unit.
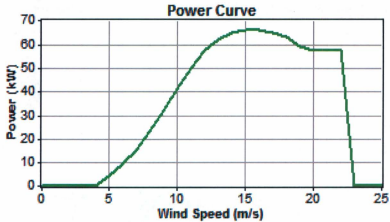
Figure 2.3: Windmatic Wind Turbine Power Curve

2.3.2 North Wind 100 Wind Turbine (100 kW)

NW100 is a 103 kW AC power generating wind turbine which is manufactured by Northern Power Incorporation. Its operating life span is 20 years and has a hub height of 37 m.
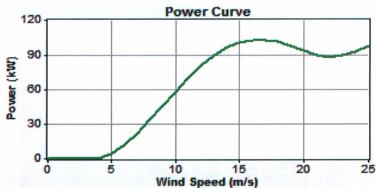
Figure 2.4: NW100 Wind Turbine Power Curve

The power curve of this wind turbine provided by the manufacturer is depicted in Figure 2.4. The capital cost (including transportation & installation) and replacement cost are $ 550,000 and 480,000 respectively. The O & M cost chosen as $3600 per year for each unit. Three NW100 wind turbines are installed in Ramea power system.

2.3.3 Diesel Generator (925 kW)

Although, there are three diesel generators on site, one of them is running continuously while the other two are operated in standby mode. Therefore, only one 925 kW is selected for purposes of calculating the optimal size of the propose FESS. The capital and replacement cost are $ 100,000 and $ 80,000 respectively for single unit. From [37], the O&M cost has been found as $ 5 per hour. Its operating time is culled as 10,000 hours from the same reference. However, 30% is taken as the minimum load ratio, which represents that minimum 277.5 kW load is required for appropriate functioning of the diesel generator. In order to define the generator efficiency, two parameter values should be assigned; one is the intercept coefficient and another is the slope of the efficiency curve.
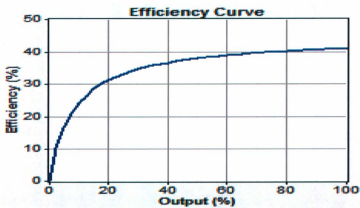
Figure 2.5: Diesel Generator Efficiency Curve

2.3.4 Hydrogen Generator

There are four hydrogen generators, each of 62.5 kW rated power, planned to be operated in both continuously and stand-by modes. Their fuel is compressed hydrogen supplied and stored in special tank. The 250 kW hydrogen generators' capital, replacement and O&M cost are $200,000, $150,000 and $5 per hour, respectively. Like the diesel generators the lifetime and minimum load ratio of the hydrogen generators are 10,000 hours [37] and 30%. Furthermore, the values of intercept coefficient and the slope have been gleaned as 0.003238 L/hr/rated kW and 0.1629 L/hr/output kW. After considering all these values the efficiency of the hydrogen generators become similar to the curve in Figure 2.5.
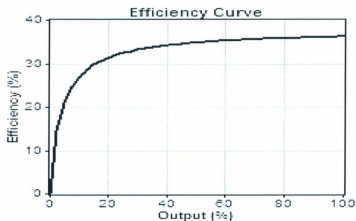
Figure 2.6: Hydrogen Generator Efficiency Curve

2.2.5 Electrolyzer

A 200 kW rated electrolyzer is soon to be installed and integrated as part of Ramea hybrid power system. The life span of this electrolyzer is selected as 5 years [38-40], efficiency is 75%, and minimum load ratio is 30%. As reported by NL Hydro [36], the capital, replacement and the O&M costs have been estimated at $ 150,000, $ 120,000 and $ 600 per year. As this device is to be connected to the AC bus, the AC type electrolyzer has been selected.
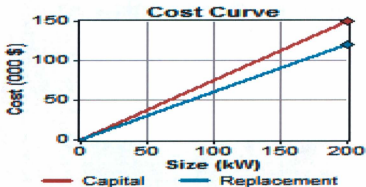
Figure 2.7: Electrolyzer Cost Curve

2.2.6 Hydrogen Tanks

Three hydrogen tanks have been set up in Ramea with a collective volume of 1000 Nm^3 and storage capacity of 84 kg. Their capital and replacement costs are $100,000 and $70,000 respectively, with no expenditure for O&M [36]. Ten years has been culled as their operation duration [38-40]. In HOMER software, it has been considered that there is

no hydrogen initially in the tank. However, there is no requirement for maintaining the year-end tank level.

Figure 2.8: Hydrogen Tanks in Ramea

2.2.7 Primary Load

The island of Ramea has 300 settlements including houses, school, churches, fish plants, commercial institutions and recreational buildings. The hourly load data throughout the year have been found from [36] and input to HOMER software tool. The primary load window reveals that the daily average energy consumption is 11,728 kWh. Moreover, the average and peak load of this region are recorded as 489 kW and 1091 kW sequentially. The property of load variations can be elucidated by two terminologies; one is day-to-day variations and another is time step-to-time step variations. The former term represents the standard deviation in the sequence of daily averages and the latter term recounts the standard deviation in the difference between the hourly data and the average daily profile. They can be expressed numerically as 8.14% and 7.86% respectively. The load factor is reported as 0.448 and can be defined as the ratio of average load demand to the peak load. Besides the average daily energy consumption, additional four nearby values such as

10,500 kWh/d, 11, 000 kWh/d, 12,000 kWh/d and 12,500 kWh/d have been considered for sensitivity analysis. The hourly load profile and the scaled daily profiles are shown in Figure 2.6 and 2.7 respectively.
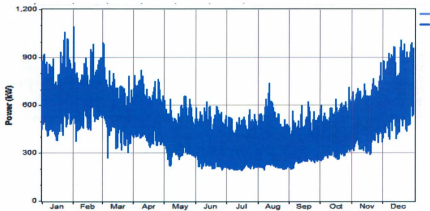
Figure 2.9: Load profile of Ramea
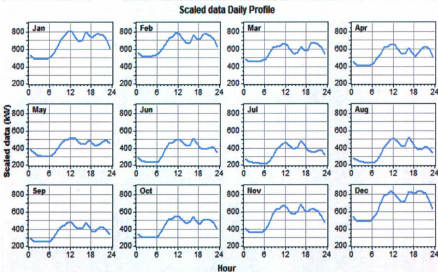
Figure 2.10: Daily Load profile of Ramea

2.2.8 Smart Energy 25 Flywheel

The smart energy 25 flywheel for the short time energy back up is selected which has a capital cost & a replacement cost of $10,000 and O & M cost of almost zero [41]. The Smart Energy 25 flywheel is the 4th-generation advanced energy storage solution designed to meet the requirements of demanding utility grid applications. It features a long-life, low-maintenance design, highly cyclic (charge-discharge) capability, and zero fuel consumption or CO_2 or other emissions. An array of Smart Energy flywheel units can be configured to form a Smart Energy Matrix plant, which can store and return megawatts of energy to maintain grid reliable and stable operation.

Figure 2.11: Beacon Smart Energy 25 Flywheel

The Smart Energy 25 flywheel offers many technical and performance advantages, including:

Highly cyclic capability: Smart Energy 25 flywheels are designed for hundreds of thousands of charge-discharge cycles over their 20-year life, making them ideally suited to the frequency regulation function.

Smart Grid attributes: Smart Energy 25 flywheels and Smart Energy Matrix plants are interactive systems that can be monitored and operated remotely as part of an smart grid design.

20-year design life: Smart Energy 25 flywheels are designed and built for 20 years of virtually maintenance-free operation.

Sustainable technology: Smart Energy 25 flywheels are emissions-free, do not require fuel, and contain no hazardous chemical materials, simplifying permitting and avoiding potential ground contamination issues.

The Smart Energy 25 flywheel system includes a rotating carbon-fiber composite rim, levitated on hybrid magnetic bearings operating in a near-frictionless vacuum-sealed environment. The rim itself is fabricated from a patented combination of high-strength, lightweight fiber composites, including graphite and fiberglass combined with resins, which allow the flywheel to rotate at high speeds (16,000 rpm) and store large amounts of energy as compared to flywheels made from metals. To reach its operational speed, the system draws electricity from the grid to power a permanent magnet motor. As the rim spins faster, it stores energy in the form of kinetic energy. The flywheel can spin for very extended periods with great efficiency because friction and drag are reduced by the use of magnetic bearings in a vacuum-sealed environment. Because it incurs low friction, little power is required to maintain the flywheel's operating speed. When a grid operator sends a signal that requests the system to absorb power, the Smart Energy Matrix uses power from the grid to drive the motor/generator, which in turn spins up the flywheel. When a signal is sent for electrical power to be provided, the momentum of the spinning flywheel

drives a generator and the kinetic energy is converted into electrical energy for release to the grid.
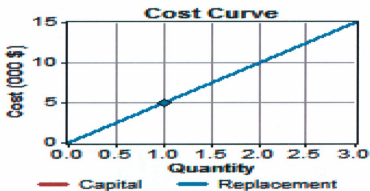
Figure 2.12: Smart Energy 25 Flywheel Cost Curve

2.4 Available Resources

The only renewable resource used for the energy production in Ramea is wind. No other green energy source proves more potentiality than wind in or nearby to this region. The daily solar insolation in this territory has been found as 3.174 kWh/m^2 and the clearness index as 0.453 [42] which are inadequate. As a consequence, no PV panel has been set up for utilizing the solar energy. As stated before wind, diesel and hydrogen are the fuels for three types of generation. Hydrogen is produced by the electrolyzer which behaves like a load for the power generation systems. This section will explicate the wind and diesel as external sources to the power system. However, internally generated hydrogen will come up in further discussion.

2.4.1 Wind Energy

The 8760x60 data points with a sampling time of one minute, wind speed throughout the year have been extracted from [36]. These data points can be validated considering two factors, such as the altitude of Ramea and the anemometer height from ground. In this occasion, the altitude of Ramea is reported as 0 m (above sea level) [43] and the anemometer height is set at 10 m. After inserting all the data, HOMER software automatically calculates the annual average wind speed as 6.08 m/s. In order for sensitivity analysis 5.5 m/s and 6.5 m/s have been introduced. Weibull shape factor (k), autocorrelation factor, diurnal pattern strength and hour of peak wind speed are the terminologies belong to the advanced parameters and play important roles controlling the conversion of 8760 hourly values from 12 monthly values in the table. The k denotes the width of the wind speed distribution over the year. The autocorrelation factor indicates the dependency of one hour's wind speed with that of the previous hour. The diurnal pattern strength refers to the relationship between the wind speed and the time of the day. The hour of peak wind speed simply means the time of the day when it remains the windiest on average throughout the year. In this instance the values of these advanced parameters are 2.02, 0.947, 0.0584 and 16 respectively. Several wind resource profiles are uncovered through Figure 2.13 - 2.15 as follows
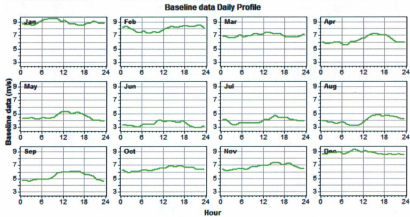
Figure 2.13: Daily Wind Speed Profile of Each Month of the Year
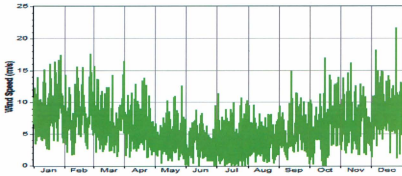
Figure 2.14: Minute Wind Speed Profile
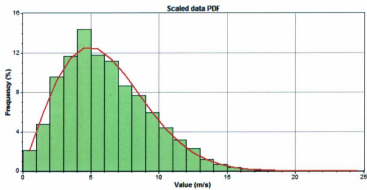
Figure 2.15: Wind Speed Probability Distribution Function

2.4.2 Diesel Energy

Although diesel has harmful emissions, it has been a versatile used fuel so far. Its most important advantage is the high energy density. The regular diesel price can be found from any gas station but most likely the diesel is cheaper when bought in a bulk amount to feed the generator. The realistic diesel price has been found from [36] as $ 1.00 per Litre. But for performing the sensitivity analysis other quantities such as $ 0.8 per Litre, $ 1.2 per Litre and $ 1.4 per Litre have been considered. Lower heating value, density, carbon content and sulfur content are the parameters used to elucidate the properties of any kind of fuel in HOMER software. In the case of diesel those values are designated as 43.2 MJ/kg, 820 kg/m, 88% and 0.33% respectively.

2.5 Simulation of Flywheel Energy Storage System (FESS) in HOMER Software

Using HOMER software two separate sets of simulations have been conducted. One set is simulated without the FESS, and the other is simulated with the FESS. The following figures show the complete system with and without FESS.

2.5.1 Simulation without FESS
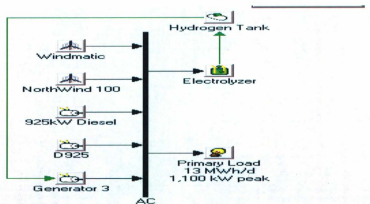
(a) Ramea hybrid power system without FESS

Cost Summary | Cash Flow | **Electrical** | WM15S | MW100 | D925 | Gen3 | Electrolyzer | Hydrogen | H2 Tank | Emissions | Time Series

Production	kWh/yr	%
Wind turbines	1,583,270	30
925kW Diesel	3,540,199	68
Generator 3	83,191	2
Total	5,206,660	100

Consumption	kWh/yr	%
AC primary load	4,644,589	92
Electrolyzer load	384,252	8
Total	5,028,841	100

Quantity	kWh/yr	%
Excess electricity	170,032	3.27
Unmet electric load	1,781	0.04
Capacity shortage	1,781	0.04

Quantity	Value
Renewable fraction	0.238
Max. renew. penetration	65.5 %

(b) Output of electrical properties without FESS

Cost Summary | Cash Flow | Electrical | WM15S | MW100 | D925 | **Gen3** | Electrolyzer | Hydrogen | H2 Tank | Emissions | Time Series

Quantity	Value	Units
Hours of operation	752	hr/yr
Number of starts	43,848	starts/yr
Operational life	53.2	yr
Capacity factor	3.80	%
Fixed generation cost	8.75	$/hr
Marginal generation cost	0.00	$/kWh

Quantity	Value	Units
Electrical production	83,191	kWh/yr
Mean electrical output	111	kW
Min. electrical output	75.0	kW
Max. electrical output	250	kW

Quantity	Value	Units
Hydrogen consumption	7,223	kg/yr
Specific fuel consumption	0.087	kg/kWh
Fuel energy input	240,751	kWh/yr
Mean electrical efficiency	34.6	%

(c) Output of diesel generator without FESS

Cost Summary | Cash Flow | Electrical | WM15S | **MW100** | D925 | Gen3 | Electrolyzer | Hydrogen | H2 Tank | Emissions | Time Series

Quantity	Value	Units
Hours of operation	8,760	hr/yr
Number of starts	1	starts/yr
Operational life	10.3	yr
Capacity factor	43.7	%
Fixed generation cost	20.3	$/hr
Marginal generation cost	0.183	$/kWh

Quantity	Value	Units
Electrical production	3,540,199	kWh/yr
Mean electrical output	404	kW
Min. electrical output	278	kW
Max. electrical output	925	kW

Quantity	Value	Units
Fuel consumption	969,505	L/yr
Specific fuel consumption	0.274	L/kWh
Fuel energy input	9,538,932	kWh/yr
Mean electrical efficiency	37.1	%

(d) Output of hydrogen generator without FESS

Fig.2.16 Simulation results of Ramea Hybrid Power System
in HOMER without FESS

2.5.2 Simulation with FESS
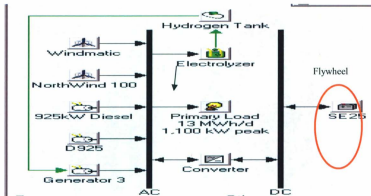
(e) Ramea hybrid power system with FESS

Cost Summary	Cash Flow	Electrical	WM15S	NW100	D925	Gen3	Battery	Converter	Electrolyzer	Hydrogen	H2 Tank	Emissions	Tim...

Production	kWh/yr	%
Wind turbines	1,583,270	32
925kW Diesel	3,382,541	68
Generator 3	38,638	1
Total	5,005,048	100

Consumption	kWh/yr	%
AC primary load	4,644,619	96
Electrolyzer load	180,313	4
Total	4,824,933	100

Quantity	kWh/yr	%
Excess electricity	96,912	1.94
Unmet electric load	1,752	0.04
Capacity shortage	1,752	0.04

Quantity	Value
Renewable fraction	0.272
Max. renew. penetration	76.6 %

(f) Output of electrical properties with FESS

Cost Summary	Cash Flow	Electrical	WM15S	NW100	D925	Gen3	Battery	Converter	Electrolyzer	Hydrogen	H2 Tank	Emissions	Tim...

Quantity	Value	Units
Hours of operation	317	hr/yr
Number of starts	18,727	starts/yr
Operational life	1.26	yr
Capacity factor	1.77	%
Fixed generation cost	8.75	$/hr
Marginal generation cost	0.00	$/kWh

Quantity	Value	Units
Electrical production	38,838	kWh/yr
Mean electrical output	123	kW
Min. electrical output	75.0	kW
Max. electrical output	250	kW

Quantity	Value	Units
Hydrogen consumption	3,345	kg/yr
Specific fuel consumption	0.086	kg/kWh
Fuel energy input	111,487	kWh/yr
Mean electrical efficiency	34.8	%

(g) Output of diesel generator with FESS

Cost Summary | Cash Flow | Electrical | WM15S | NW100 | DS25 | Gen3 | Battery | Converter | Electrolyzer | Hydrogen | H2 Tank | Emissions | Tim...

Quantity	Value	Units
Hours of operation	8,760	hr/yr
Number of starts	1	starts/yr
Operational life	10.3	yr
Capacity factor	41.7	%
Fixed generation cost	20.3	$/hr
Marginal generation cost	0.183	$/kWh

Quantity	Value	Units
Electrical production	3,382,941	kWh/yr
Mean electrical output	386	kW
Min. electrical output	278	kW
Max. electrical output	925	kW

Quantity	Value	Units
Fuel consumption	933,849	L/yr
Specific fuel consumption	0.276	L/kWh
Fuel energy input	9,189,063	kWh/yr
Mean electrical efficiency	36.8	%

(h) Output of hydrogen generator with FESS

Fig.2.17 Simulation results of Ramea Hybrid Power System in HOMER with FESS

2.6 Observations and Comparison of Simulation Result

The total system expenditure can be identified by the Net Present Cost (NPC). Figure 2.18 explain the system NPC by pointing out the capital, replacement, operating, fuel costs and salvage values of individual components with and without FESS. As the diesel generator runs continuously 8760 hours in a year, it consumes large amount of diesel. Therefore, the fuel cost is remarkably high for the diesel generator. Like fuel cost, the O&M cost is again the highest for the diesel generators. The salvage value refers to the amount that can be compatible to market price at that instant of any component or the whole system after a certain years of operation. In order to determine the total system cost, this salvage amount is deducted from the capital, replacement, O&M and fuel costs altogether. Moreover, the Cost of Energy (COE) of this system has been reported as 0.302 $/kWh.
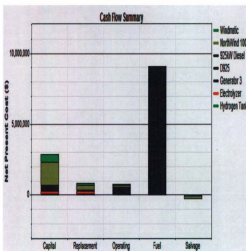
(a)
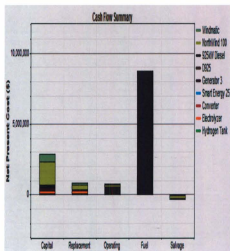
(b)

Fig.2.18 Net percent cost curves of Ramea hybrid Power System in HOMER
(a) with and (b) without FESS
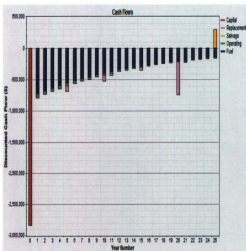
(c)
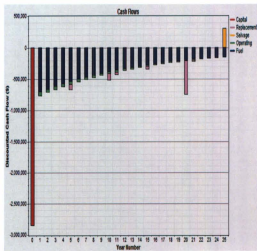
(d)

Fig.2.19 Discounted cash flow curves of Ramea hybrid Power System
in HOMER (c) with and (d) without FESS

Component	Capital ($)	Replacement ($)	O&M ($)	Fuel ($)	Salvage ($)	Total ($)
Windmatic	540,000	108,536	83,906	0	-58,038	674,403
NorthWind 100	1,650,000	372,123	125,859	0	-198,989	1,948,993
925kW Diesel	100,000	59,842	510,427	9,011,031	-8,353	9,672,948
D925	100,000	0	3,146	41,008	-14,519	129,635
Generator 3	200,000	0	43,817	0	-14,648	229,170
Electrolyzer	150,000	221,064	6,992	0	0	378,056
Hydrogen Tank	100,000	53,674	0	0	-6,449	147,225
System	2,840,000	815,239	774,147	9,052,039	-300,995	13,180,430

(e)

Component	Capital ($)	Replacement ($)	O&M ($)	Fuel ($)	Salvage ($)	Total ($)
925kW Diesel	100,000	59,842	510,427	8,679,409	-8,353	9,341,325
D925	1,650,000	372,123	125,859	0	-198,989	1,948,993
Generator 3	100,000	59,842	510,427	8,679,409	-8,353	9,341,325
Smart Energy 25	100,000	0	3,030	39,930	-14,527	128,433
Converter	200,000	0	18,471	0	-22,162	196,309
Electrolyzer	5,000	1,292	0	0	-691	5,601
Hydrogen Tank	100,000	53,674	0	0	-6,449	147,225
System	2,845,000	816,531	748,684	8,719,339	-309,208	12,820,347

(f)

Fig.2.20 Break down of Net Percent Cost of Ramea hybrid Power System in
HOMER (e) without and (f) with FESS

From figure 2.19 and 2.20 one can see the discounted cash flow curve and break down of
net percent cost of Ramea hybrid power system with and without FESS respectively.
From the break down cost summary it is clear that with the addition of a FESS the total
system cost is reduced from $13,180,430 to $12, 800347.

57

(g)

(h)
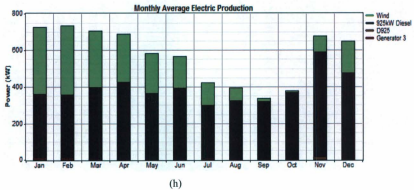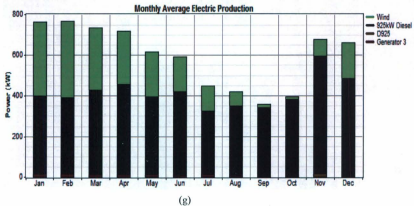
Fig.2.21 Monthly Average Electric Production of Ramea hybrid Power System in HOMER (g) without and (h) with FESS

(i)

(j)
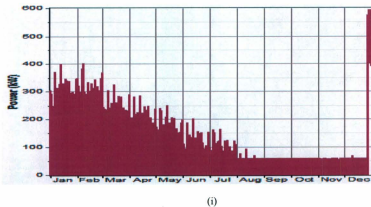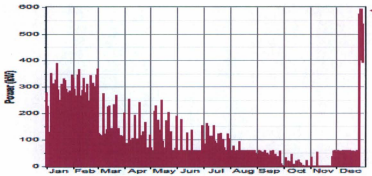
Fig.2.22 Excess Electricity of Ramea hybrid Power System in HOMER
(i) without and (j) with FESS

Figure 2.21 and 2.22 shows the monthly average electricity generation and excess electricity for Ramea. Excess electricity curves clearly shows that, with FESS, excess electricity is reduced significantly.
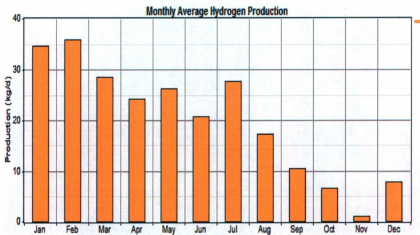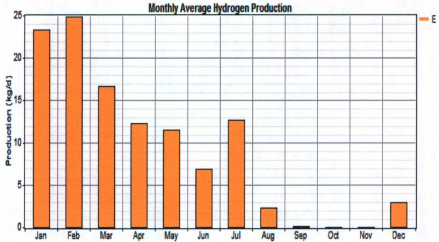
(ii)

Fig.2.23 Monthly Average Hydrogen Production of Ramea hybrid Power
System in HOMER (i) with and (ii) without FESS

(iii)

(iv)
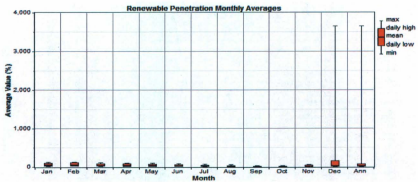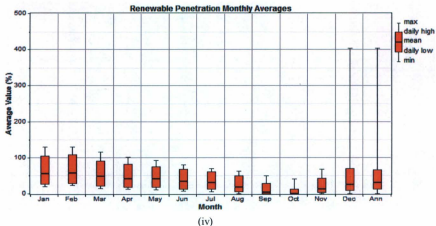
Fig.2.24 Renewable Penetration Monthly Average of Ramea hybrid Power
System in HOMER (iii) without and (iv) with FESS

Figure 2.23 and 2.24 shows the monthly average Hydrogen production and monthly average renewable penetration of Ramea Hybrid Power System. From hydrogen production graph it is seen that with FESS the hydrogen production is reduced because the number of switching of the hydrogen generator is reduced. Also from renewable penetration graph, it clearly shows that with and addition of FESS the penetration is much better in the system which is expected.
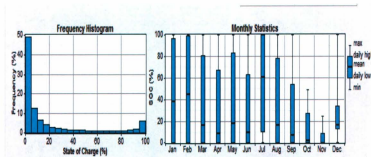
Fig.2.25 State of Charge curve of FESS of Ramea hybrid Power System in HOMER

From Figure 2.25, it can be seen that, the state of charge of the FESS of Ramea Hybrid Power System. At the end of the year the state of charge is little bit lower than the beginning of the year.

(i)
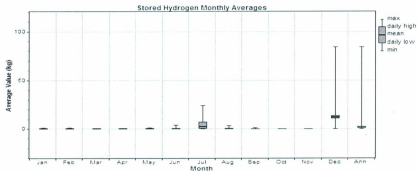
(ii)

Fig.2.26 Stored Hydrogen comparison of Ramea hybrid Power System in HOMER (a) without and (b) with Flywheel

Figure 2.26 concludes that, with the FESS in Ramea Hybrid system, the stored hydrogen can be increased.

2.6.1 Green House Gas Emissions by the Hybrid Power System

Green House Gas (GHG) emission has become an important issue nowadays. The foremost objective of exploiting the renewable resources and introducing hybrid power systems is to ensure healthier environment. Before utilizing the three 100 kW wind turbines and electrolyzer, hydrogen tank and hydrogen generators, the condition was far worse in terms of pollutant quantity. After introducing those components, the conditions have been improved, although the carbon dioxide emission is still too high. The second highest pollutant is nitrogen oxides, but with the addition of an FESS, the green house gas emissions is reduced significantly as shown in figure 2.27

Pollutant	Emissions (kg/yr)
Carbon dioxide	2,556,759
Carbon monoxide	6,358
Unburned hydrocarbons	704
Particulate matter	479
Sulfur dioxide	5,135
Nitrogen oxides	56,734

Pollutant	Emissions (kg/yr)
Carbon dioxide	2,462,824
Carbon monoxide	6,101
Unburned hydrocarbons	676
Particulate matter	460
Sulfur dioxide	4,946
Nitrogen oxides	54,439

Fig.2.27 Green House gas emission comparison of Ramea hybrid Power System in HOMER (a) without and (b) with Flywheel

(a)   (b)

Results of previous observations are summarized in the Table I.

Table I

Considering Factors		Without Flywheel	*With Flywheel*
Electrical Properties	Excess Electricity	3.27%	*1.94%*
	Renewable Fraction	0.238	*0.272*
	Maximum Renewable Penetration	65.5%	*76.6%*
Diesel Generator (D925)	Electricity Generation	3540199 kWh/yr	*3382941 kWh/yr*
	Fuel Consumption	965505 L/yr	*933848 L/yr*
Hydrogen Generator (Gen3)	Hours of Operations	752/yr	*317/yr*
	Number of Starts	43848/yr	*18727/yr*
	Hydrogen Consumption	7223 kg/yr	*3345 kg/yr*
	Mean Electrical efficiency	34.6%	*34.8%*
	Operational Life	53.2 yr	*126 yr*
Emission	Carbon Dioxide	2552953 kg/yr	*2459094 kg/yr*
	Carbon Monoxide	6349 kg/yr	*6092 kg/yr*
	Unburned Hydrocarbon	703 kg/yr	*675 kg/yr*

2.8 Summary

In this chapter, descriptions of various components of Ramea hybrid power system are presented. Explanations of the economic and electric properties of Ramea Wind-Hydrogen-Diesel Hybrid power system have been provided by using HOMER software.

Most of the necessary data has been provided by Newfoundland Hydro. Capital, replacement and O&M costs have been assigned for each component along with their lifetime. This is to be noted that these three costs are the most important input that HOMER software deals with. Comparisons of various results from the HOMER simulations are also presented in this chapter. The observations are carried out for two conditions, normally with FESS and without. Excess electricity, maximum renewable penetration, fuel consumption, number of starts per year, operational life and emissions of different hazardous chemicals were taken as considering factors. In this research we have tried to prove that an addition of a flywheel energy storage system to the existing power system of Ramea will be very effective. 'HOMER' software simulation output shows that with the addition of flywheel energy storage system (FESS) will reduce the fuel consumption of the diesel generator and hydrogen generator, excess electricity is less, emissions of hazardous chemical components have been reduced, also number of switching of the generators have been decreased by 50%, and the life cycle has been increased for the generator. Furthermore, it has been observed that use of a single 25kWh FESS could increase the maximum renewable penetration and the hours of operation of the generators per year have been decreases.

Chapter 3

Dynamic modeling and Simulation of Ramea Hybrid Power System with Flywheel Energy Storage

3.1 Concept of Hybrid Power System

Renewable energy sources like solar energy, wind energy, or micro hydropower has potential and capacity to meet power demands for remote areas. The abundant energy available in nature can be harnessed and converted to electricity in a sustainable way to supply the necessary power to isolated loads which operate in stand-alone modes. Using renewable energy sources for generating power in remote areas can reduce the cost of transported fuel among with minimizing the impact on the environment. The availability of renewable energy sources has daily and seasonal patterns which result in difficulties in regulating the output power to meet the demand constrains of fixed voltage and frequency. Combining the renewable energy generation with conventional diesel power generation can improve the reliability and stability of distributed generation units. These

types of electric power generation system, which consists of renewable energy and fossil fuel generators together with an energy storage system and power conditioning system, is known as a hybrid power system. A hybrid power system can provide day long good quality of electricity to the load and offers better efficiency, flexibility of planning and environmental benefits compared to the diesel generator stand-alone system. The operational and maintenance costs of the diesel generator can be decreased as a consequence of improving the efficiency of operation and reducing the operational time which implies less fuel usage. Such power system gives the opportunity for expanding its capacity in order to cope with increasing demands in the future. This can be done by increasing the rated power of diesel generator or renewable generator.
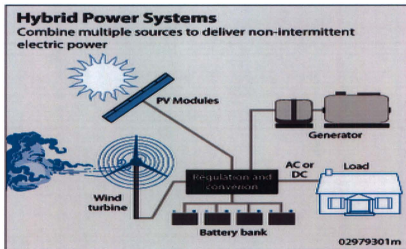
Figure 3.1: Typical Hybrid Power System

For domestic consumers in remote areas that are not served by the main electrical grid network, diesel generators are the usual choice for electric power supply. As a result,

plenty of servicing and maintenance need to be done for these diesel generators. Thus, researchers have come out with ideas of introducing wind turbines working together with the diesel generators to form a hybrid power system. This chapter utilizes the MATLAB/SIMULINK software in the modeling of such wind-diesel hybrid power system with FESS for a stand-alone system in the remote location of Ramea, Newfoundland. This addition of wind energy inputs in conjunction with the diesel generators facilities saving fuel. In addition, short term energy storage FESS is proposed to maintain the load demand and frequency regulation during sudden changes in load demands or wind speed.

A number of remote and rural areas in the world, a noteworthy number of domestic consumers, farms and small businesses are not connected to a utility system. This is exceptionally real in the developing countries, where large distances and the lack of capital are major obstacles to the development of utility systems. This can be found in developed countries such as Great Britain, where there are a significant number of consumers without a grid supply. Since the remote areas are normally not connected to the grid supply, their usual method of electricity generation is diesel generating sets. These have the advantage of being able to deliver the required power whenever it is necessary. However, they also suffer from a number of drawbacks. Diesel generator engines are inherently noisy and expensive to run, especially for consumers in rural areas, where fuel delivery costs can be high. Moreover, small consumers always have a low load factor; this in turn reduces the overall efficiency and increases percentage maintenance costs. Hence, it is necessary to explore possibilities of combining a wind generator with diesel generators in order to reduce the running cost per kWh. As the wind speed and the

load have tendencies to change, a short term back up energy is necessary to ensure the stability under frequency fluctuations.

3.3 Modeling of Wind Energy Conversion Systems

Wind energy conversion systems associated with various components and devices like wind turbine blades, wind generators, switching devices, transformers converters etc. In the following section detailed model of a wind power generation is presented.

3.4 Wind Power Generation System Model

The principle components of a modern wind turbine are the tower, the rotor and the nacelle, which accommodates the transmission mechanisms and the generator, and for horizontal-axis devices, the yaw system for steering in response to changes in wind direction. Switching and protection systems, lines, transformers and networks, are required delivering the generated power. In response to the external influences, a unit for operational control and regulation must adapt the flow of energy from the system to its demands. The block diagram given in Figure 3.2, shows links between the most important components and the associated energy conversion stages, may serve as the basis for later detailed sections. This figure gives an idea about the role of control and supervisory actions on the wind turbine operation. Moreover, the central position occupied by the generator becomes particularly significant. Figure 3.3 shows the different components and their location in a wind turbine system. The following section explicates the physical behavior of a wind energy conversion system (WECS) and conversion of the mechanical energy to the electrical energy by means of generators.
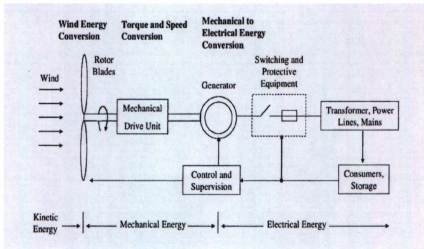
Figure 3.2: Energy Transfer in a Wind Energy Conversion system

3.5 Components of Wind Power Plants

The dynamic models of WMl5S and NWlOO wind turbines are employed to model the 65 kW two squirrel-cage induction generators-based WECS and the 100 kW direct-drive permanent magnet synchronous generator-based WECS. Before analyzing the dynamic behavior, it is more practical to compute their steady state behaviors first and then incorporating them with other components.

3.5.1 Wind Turbine Rotor

The relation between wind velocity and the rotor output power of a wind turbine can be expressed as:

$$P_{ro} = 0.5 \rho A_{SA} C_p(\lambda, \beta) v_w^3 \quad \dots \dots \dots \dots \dots \dots \dots \dots \dots \dots \dots \dots \dots \dots \dots \dots \dots \dots \dots \dots \quad (3.1)$$

Tip speed ratio λ is the quotient of linear speed of the tip of the blades to the rotational speed of WT and it is expressed as

$$\lambda = \frac{\omega_m R_t}{v_w} \quad \dots\dots\dots\dots\dots\dots\dots\dots\dots\dots\dots\dots\dots\dots\dots\dots\dots\dots\dots\dots\dots\dots (3.2)$$

A generalized non-linear relation between performance coefficient and tip speed ratio of a WT is developed in [3]. The effects of the different $C_p - \lambda$ curves for various types of wind turbines are very small and negligible, while the electrical behavior of a system is of a great interest [4]. Therefore, the analytical approximation of the $C_p - \lambda$ characteristics presented in [3] is considered for rotor modeling and is expressed as

$$C_p(\lambda, \beta) = 0.5176(\frac{116}{\lambda_i} - 0.4\beta - 0.5)e^{\frac{-21}{\lambda_i}} + 0.0068\lambda \dots\dots\dots\dots\dots\dots\dots\dots\dots\dots\dots (3.3)$$

and

$$\frac{1}{\lambda_i} = \frac{1}{\lambda + 0.08\beta} - \frac{0.035}{\beta^3 + 1} \quad \dots\dots\dots\dots\dots\dots\dots\dots\dots\dots\dots\dots\dots\dots\dots\dots\dots (3.4)$$

3.5.2 Rotor Blades

Different types of materials like aluminum, steel, titanium, fiber composite material (glass, carbon and aramide fibers) and wood [53] are generally used for manufacturing wind turbine blades. The most important material properties for wind turbine blades are specific weights, strength limit, tearing length, modulus of elasticity related to the specific weight and allowable fatigue stress after 107 to 108 load cycles. However, material cost, production cost and cost of development involved are also significant factors. From the specification sheets collected from manufacturer websites, it has been found that the wind turbines in Ramea have fiber reinforced composite blades. These materials are currently

being used in almost all lightweight structures. Even in large commercial aircraft, fiber reinforced materials increasingly prevail. Glass, carbon and organic aramide fibers are presently available materials found in the marketplace. The fibers are available in highly varying qualities, from high-quality aero-space quality down to low-grade fiber material for simple fairing structures. The fatigue strength of organic aramide fibers has not been tested yet completely and hence they cannot be taken into consideration for rotor blades. The most widely used fiber is glass fiber.

3.5.3 Electrical Generation Systems

Different kinds of generators are used in WECS including doubly-fed induction generator, permanent magnet synchronous generator and squirrel cage induction generator. WM15S and NW100 wind turbines used in Ramea employ squirrel cage induction generator and permanent magnet synchronous generator respectively. The AC generators used in WTs are discussed in the following sections.

3.5.4 Squirrel Cage Induction Generator

A three phase squirrel cage induction generator has three identical windings that are symmetrically distributed around the inner surface of a laminated cylindrical shell called the stator. The laminated rotor inside carries a winding consisting of bars connected to two shorting rings at both ends. This rotor can be characterized to be adapted to any number of stator poles. When the balanced stator windings wound for p number of pole pairs and displaced in space by 120 electrical degrees and the applied torque creates a field rotation in the air gap, ns, then a three phase voltage will be induced in the stator

winding having frequency, f. The relationship between pole pairs, frequency and the field rotation can be expressed as follows [47]

$$N_s = \frac{120f}{p} \dots\dots\dots\dots\dots\dots\dots\dots\dots\dots\dots\dots\dots\dots\dots\dots\dots\dots\dots\dots\dots (3.5)$$

Here N_s is expressed in rad/s and is known as the synchronous speed of the induction generator. The resultant air-gap flux, rpm is set up by the combined action of the stator and the rotor magneto-motive force (mmf). This synchronous rotating flux induces a counter emf E, in the stator phase winding. The stator terminal voltage V differs from this counter emf E, by the stator leakage impedance drop. The stator emf phasor equation is then

$$\bar{V}_1 = \bar{E}_1 + I_1(R_s + JX_{ls}) \dots\dots\dots\dots\dots\dots\dots\dots\dots\dots\dots\dots\dots\dots\dots\dots\dots\dots\dots\dots (3.6)$$

The circuit representation of equation 3.6 is shown in Figure 3.2. The current I_1 in the stator winding can be resolved into an exciting component I0 and a compensating load component current I'$_2$. The load component current I'$_2$ counteracts the rotor mmf, thereby demanding power from source. The exciting component Io can be resolved into a core loss component I$_e$, in phase with the stator induced emf E, and a magnetizing component I$_m$, lagging behind the induced emf E, by 90°. This is the magnetizing component which sets up the air gap flux.

The asynchronous machine block in MATLAB/Sim Power Systems/ Machines tool box operates either as motor or a generator mode. The mode of operation is dictated by the sign of the mechanical torque. For positive Tm the block acts as a motor and for negative Tm it operates as a generator.
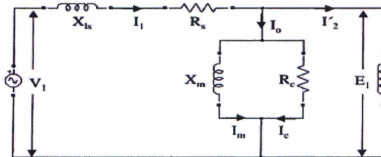
Figure 3.2: Per-phase Stator Circuit Model of a Three Phase Induction Motor [44]

The electrical part of the machine is represented by a fourth order state space model and the mechanical part by a second order system. All electrical parameters and variables are referred to the stator. These are denoted by the prime signs in the machine equations. All stator and rotor quantities are in the arbitrary two axis d-q reference frame. The expressions related to d-q axis representation of an asynchronous generator are stated below [48]
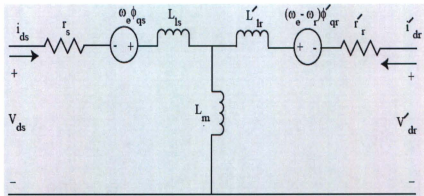
(a) d-axis
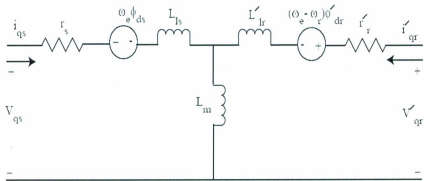
(b) *q*-axis

Figure 3.3: Equivalent circuit representation of an induction machine: (a)

d-axis, (b) *q*-axis.

The induction machine voltage equations are expressed as

$$V_{ds} = r_s i_{ds} - \omega_e \varphi_{qs} + \frac{d\varphi_{ds}}{dt} \quad \text{..} \quad (3.7)$$

$$V_{qs} = r_s i_{qs} + \omega_e \varphi_{ds} + \frac{d\varphi_{qs}}{dt} \quad \text{..} \quad (3.8)$$

$$V'_{dr} = r'_r i'_{dr} - (\omega_e - \omega_r)\varphi'_{qr} + \frac{d\varphi'_{dr}}{dt} \quad \text{..} \quad (3.9)$$

$$V'_{qr} = r'_r i'_{qr} + (\omega_e - \omega_r)\varphi'_{dr} + \frac{d\varphi'_{qr}}{dt} \quad \text{..} \quad (3.10)$$

Rearranging equations

$$\varphi_{ds} = \int [V_{ds} - r_s i_{ds} + \omega_s \varphi_{qs}] dt \quad \ldots\ldots\ldots\ldots\ldots\ldots\ldots\ldots\ldots\ldots\ldots\ldots \quad (3.11)$$

$$\varphi_{qs} = \int [V_{qs} - r_s i_{qs} + \omega_s \varphi_{ds}] dt \quad \ldots\ldots\ldots\ldots\ldots\ldots\ldots\ldots\ldots\ldots\ldots\ldots \quad (3.12)$$

$$\varphi'_{dr} = \int [V'_{dr} - r'_r i'_{dr} + (\omega_e - \omega_r)\varphi'_{qr}] dt \quad \ldots\ldots\ldots\ldots\ldots\ldots\ldots\ldots\ldots\ldots\ldots \quad (3.13)$$

$$\varphi'_{qr} = \int [V'_{qr} - r'_r i'_{qr} + (\omega_e - \omega_r)\varphi'_{dr}] dt \quad \ldots\ldots\ldots\ldots\ldots\ldots\ldots\ldots\ldots\ldots\ldots \quad (3.14)$$

The mechanical part can be represented as below:

$$\frac{d}{dt}\omega_m = \frac{1}{2H}(T_e - F\omega_m - T_m) \quad \ldots\ldots\ldots\ldots\ldots\ldots\ldots\ldots\ldots\ldots\ldots\ldots\ldots\ldots\ldots\ldots \quad (3.15)$$

$$\frac{d}{dt}\theta_m = \omega_m \quad \quad \quad \ldots\ldots\ldots\ldots\ldots\ldots\ldots\ldots\ldots\ldots\ldots\ldots\ldots\ldots\ldots \quad (3.16)$$

3.5.5 Permanent Magnet Synchronous Generator

The basic wind energy conversion requirements of a variable speed permanent generator are almost the same as those for a wound-field synchronous generator. The permanent magnet generator dispenses with the need for external excitation. Therefore, the output voltage, under variable speed operation, varies both in frequency and in magnitude. As a consequence, the DC-link voltage changes in an uncontrolled manner which can be controlled using a grid connected DC-AC converter.
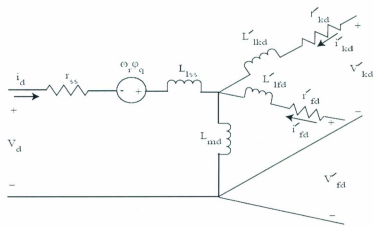
(a)
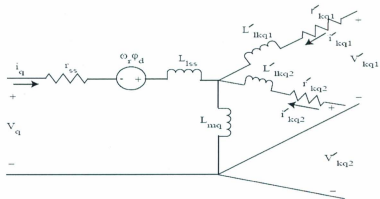
(b)

Figure 3.4: Equivalent circuit representation of a synchronous machine:
(a) *d*-axis, (b) *q*-axis.

The voltage equations in *d-q* axis rotor reference frame of synchronous machine are
expressed as [67]

$$V_d = r_{ss}i_d - \omega_r\varphi_q + \frac{d\varphi_d}{dt} \qquad .... \quad (3.16)$$

$$V_q = r_{ss}i_q + \omega_r\varphi_d + \frac{d\varphi_q}{dt} \qquad .... \quad (3.17)$$

$$V'_{fd} = r'_{fd}i'_{fd} + \frac{d\varphi'_{fd}}{dt} \qquad .... \quad (3.18)$$

$$V'_{kd} = r'_{kd}i'_{kd} + \frac{d\varphi'_{kd}}{dt} \qquad .... \quad (3.19)$$

$$V'_{kq1} = r'_{kq1}i'_{kq1} + \frac{d\varphi'_{kq1}}{dt} \qquad .... \quad (3.20)$$

$$V'_{kq2} = r'_{kq2}i'_{kq2} + \frac{d\varphi'_{kq2}}{dt} \qquad .... \quad (3.21)$$

Rearranging equations ,

$$\varphi_d = \int [V_d - r_{ss}i_d + \omega_r\varphi_q]dt \qquad .... \quad (3.22)$$

$$\varphi_q = \int [V_q - r_{ss}i_q + \omega_r\varphi_d]dt \qquad .... \quad (3.23)$$

$$\varphi'_{fd} = \int [V'_{fd} - r'_{fd}i'_{fd}]dt \qquad .... \quad (3.24)$$

$$\varphi'_{kd} = \int [V'_{kd} - r'_{kd}i'_{kd}]dt \qquad .... \quad (3.25)$$

$$\varphi'_{kq1} = \int [V'_{kq1} - r'_{kq1}i'_{kq1}]dt \qquad .... \quad (3.26)$$

$$\varphi'_{kq2} = \int [V'_{kq2} - r'_{kq2}i'_{kq2}]dt \quad \dots\dots\dots\dots\dots\dots\dots\dots \quad (3.27)$$

Flux linkages developed in the synchronous machine are expressed as

$$\varphi_d = L_d i_d + L_{md}(i'_{fd} + i'_{kd}) \quad \dots\dots\dots\dots\dots\dots\dots\dots \quad (3.28)$$

$$\varphi_q = L_q i_q + L_{mq}(i'_{kq1} + i'_{kq2}) \quad \dots\dots\dots\dots\dots\dots\dots \quad (3.29)$$

$$\varphi'_{fd} = L_{md} i_d + L_{md} i'_{kd} + (L'_{lfd} + L_{md})i'_{fd} \quad \dots\dots\dots\dots\dots \quad (3.30)$$

$$\varphi'_{kd} = L_{md} i_d + L_{md} i'_{fd} + (L'_{lkd} + L_{md})i'_{kd} \quad \dots\dots\dots\dots \quad (3.31)$$

$$\varphi'_{kq1} = L_{mq} i_q + L_{mq} i'_{kq2} + (L'_{lkq1} + L_{mq})i'_{kq1} \quad \dots\dots\dots\dots\dots\dots \quad (3.32)$$

$$\varphi'_{kq2} = L_{mq} i_q + L_{mq} i'_{kq1} + (L'_{lkq2} + L_{mq})i'_{kq2} \quad \dots\dots\dots\dots\dots\dots \quad (3.33)$$

Where, $L_d = L_{md} + L_{ls}$

and $L_q = L_{mq} + L_{lss}$

The mutual flux components for the direct and the quadrature axis are φ_{mds} and φ_{mqs}, respectively and are expressed as

$$\varphi_{mds} = L_{md}(i_d + i'_{fd} + i'_{kd}) \quad \dots\dots\dots\dots\dots\dots\dots\dots \quad (3.34)$$

$$\varphi_{mqs} = L_{mq}(i_q + i'_{kq1} + i'_{kq2}) \quad \dots\dots\dots\dots\dots\dots\dots\dots \quad (3.35)$$

The current equations are derived as

$$i_d = \frac{1}{L_{lss}}(\varphi_d - \varphi_{mds}) \quad \text{..} \quad (3.36)$$

$$i_q = \frac{1}{L_{lss}}(\varphi_q - \varphi_{mqs}) \quad \text{..} \quad (3.37)$$

$$i'_{fd} = \frac{1}{L'_{lfd}}(\varphi'_{fd} - \varphi_{mds}) \quad \text{..} \quad (3.38)$$

$$i'_{kd} = \frac{1}{L'_{lkd}}(\varphi'_{kd} - \varphi_{mds}) \quad \text{..} \quad (3.39)$$

$$i'_{kq1} = \frac{1}{L'_{lkq1}}(\varphi'_{kq1} - \varphi_{mqs}) \quad \text{..} \quad (3.40)$$

$$i'_{kq2} = \frac{1}{L'_{lkq2}}(\varphi'_{kq2} - \varphi_{mqs}) \quad \text{..} \quad (3.41)$$

The d and q axis mutual flux components now can be written as

$$\varphi_{mds} = L_{ad}(\frac{\varphi_d}{L_{lss}} + \frac{\varphi'_{fd}}{L'_{lfd}} + \frac{\varphi'_{kd}}{L'_{lkd}}) \quad \text{..} \quad (3.42)$$

$$\varphi_{mqs} = L_{aq}(\frac{\varphi_q}{L_{lss}} + \frac{\varphi'_{kq1}}{L'_{lkq1}} + \frac{\varphi'_{kq2}}{L'_{lkq2}}) \quad \text{..} \quad (3.43)$$

Where,

$$L_{ed} = \left(\frac{1}{L_{md}} + \frac{1}{L_{lss}} + \frac{1}{L'_{lfd}} + \frac{1}{L'_{lkd}} \right)^{-1} \quad \ldots\ldots\ldots\ldots\ldots\ldots\ldots\ldots\ldots\ldots \quad (3.44)$$

$$L_{eq} = \left(\frac{1}{L_{mq}} + \frac{1}{L_{lss}} + \frac{1}{L'_{lkq1}} + \frac{1}{L'_{lkq2}} \right)^{-1} \quad \ldots\ldots\ldots\ldots\ldots\ldots\ldots\ldots\ldots\ldots \quad (3.45)$$

Substituting equations

$$\varphi_d = \int [V_d - \frac{r_{ss}}{L_{lss}} (\varphi_d - \varphi_{mds}) + \omega_r \varphi_q] dt \quad \ldots\ldots\ldots\ldots\ldots\ldots\ldots\ldots\ldots\ldots\ldots \quad (3.46)$$

$$\varphi_q = \int [V_q - \frac{r_{ss}}{L_{ss}} (\varphi_q - \varphi_{mqs}) + \omega_r \varphi_d] dt \quad \ldots\ldots\ldots\ldots\ldots\ldots\ldots\ldots\ldots\ldots \quad (3.47)$$

$$\varphi'_{fd} = \int [V'_{fd} - \frac{r'_{fd}}{L'_{lfd}} (\varphi'_{fd} - \varphi_{mds})] dt \quad \ldots\ldots\ldots\ldots\ldots\ldots\ldots\ldots \quad (3.48)$$

$$\varphi'_{kd} = \int [V'_{kd} - \frac{r'_{kd}}{L'_{lkd}} (\varphi'_{kd} - \varphi_{mds})] dt \quad \ldots\ldots\ldots\ldots\ldots\ldots\ldots\ldots \quad (3.49)$$

$$\varphi'_{kq1} = \int [V'_{kq1} - \frac{r'_{kq1}}{L'_{lkq1}} (\varphi'_{kq1} - \varphi_{mqs})] dt \quad \ldots\ldots\ldots\ldots\ldots\ldots\ldots\ldots \quad (3.50)$$

$$\varphi'_{kq2} = \int [V'_{kq2} - \frac{r'_{kq2}}{L'_{lkq2}} (\varphi'_{kq2} - \varphi_{mqs})] dt \quad \ldots\ldots\ldots\ldots\ldots\ldots\ldots\ldots \quad (3.51)$$

The electromagnetic torque produced by the synchronous machine can be expressed as

$$T_{em\_SM} = \left(\frac{3}{2}\right) p_{sm} (\varphi_d i_q - \varphi_q i_d) \qquad \dots\dots\dots\dots\dots\dots\dots\dots\dots\dots\dots\dots\dots \quad (3.52)$$

The equation of motion of the rotor can be expressed as

$$\frac{d\omega_{r\_SM}}{dt} = \frac{1}{p_{SM} J_{SM}} (T_{m\_SM} - T_{em\_SM} - F\omega_{rm\_SM}) \dots\dots\dots\dots\dots\dots\dots\dots\dots\dots\dots \quad (3.53)$$

3.6 Transformer

At Ramea, the magnitude of the voltage associated with the energy produced by the wind turbines is 480 V which requires stepping up to levels adequate for transmitting to the grid. All the transformers employed in this region are 480V/4160V Y-Δ type. For consumer applications, this higher magnitude of voltage is again stepped down to a suitable magnitude of the voltage. Therefore, three phase transformer is very important to Increase or decrease the voltage magnitude. These transformers can be made either three single phase transformers connected together in a three phase bank or three windings wound in a common core. The former one is cheaper, smaller and lighter than the latter one [58].

As shown figure 3.5, the instantaneous emf induced in the primary winding is as follows.

$$e_1 = -N_1 \frac{d\phi}{dt} = N_1 \omega \varphi_m . \sin(90 + \omega t) \dots\dots\dots\dots\dots\dots\dots\dots\dots\dots\dots\dots\dots\dots\dots \quad (3.54)$$

The maximum value of e_1 is

$$E_{m1} = N_1 \omega \varphi_m \qquad \dots\dots\dots\dots\dots\dots\dots\dots\dots\dots\dots\dots\dots\dots\dots \quad (3.55)$$

Now the effective value of primary emf

$$E_1 = \frac{E_{m1}}{\sqrt{2}} = 4.44 f \varphi_m N_1 \qquad \ldots\ldots\ldots\ldots\ldots\ldots\ldots\ldots\ldots\ldots\ldots\ldots\ldots\ldots\ldots (3.56)$$

Similarly the emf in the secondary winding is

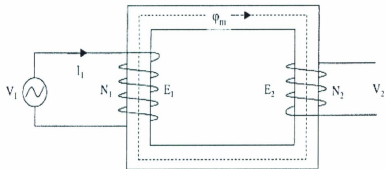$$E_1 = \frac{E_{m1}}{\sqrt{2}} = 4.44 f \varphi_m N_2$$

Figure 3.5: An Ideal Transformer

In a two winding transformer, the windings are magnetically coupled and it is hard to analyze. Therefore, the ideal transformer is converted to its equivalent circuit for the purpose of easy computation. The parameters like resistance, reactance, voltage and current can be transferred either from primary to secondary or from secondary to primary in the equivalent circuits. The magnitude of no-load circuit current is very small and it is less than 5% of the rated primary current. Hence in the equivalent circuit the no-load circuit can be neglected without making any serious error. The two winding ideal transformer is shown in Figure 3.6. And also in Figure 3.7 and 3.8 the transformer equivalent circuits are presented as referred to primary and secondary respectively.
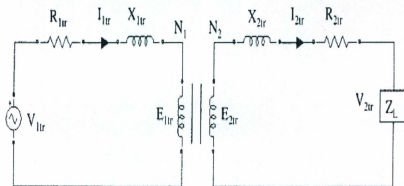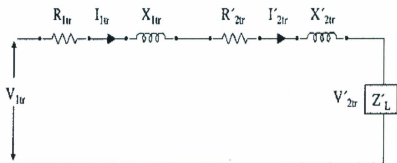
Figure 3.6: A Two Winding Transformer

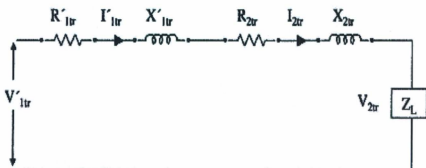Figure 3.7: Transformer Equivalent Circuit referred to Primary

Figure 3.8: Transformer Equivalent Circuit referred to Secondary

3.7 Capacitor Bank

Due to their low cost, simple structure and robust design the Squirrel cage induction generators WECS have received great attention for operating in stand-alone conditions. Although they are capable of generating active power, their main limitation is that they are unable to produce reactive power needed for their own excitation. In order to overcome such a problem, a capacitor bank is connected to the system between the generator and the load or grid. Each of the 65 kW Windmatic wind turbines at Ramea has employed a 35 kVAR/4.16kV rated capacitor bank. As the three phase capacitor bank is connected to the induction generator, an emf is induced to the machine windings due to the self excitation provided by the capacitors. The magnetizing requirements of the squirrel-cage induction generator are met by these capacitors when satisfying the following two conditions should be fulfilled.

- ❖ The rotor of the machine should have sufficient residual magnetism and
- ❖ The three phase capacitor bank should be of sufficient ratings.

After satisfying the above conditions an emf will be induced in the squirrel cage induction generator windings due to the excitation provided by the capacitors. This phenomenon is known as "Capacitor Self-Excitation". If the induced emf is sufficient, leading currents through the capacitors start to circulate.

3.8 Modeling and Simulation of 65 kW Wind Turbines (WM15S)

Earlier it has been mentioned that, at Ramea there are six squirrel cage induction generator based fixed speed wind turbines operating currently. Each of these WECS supports dual speeds, i.e. this system has two parallel generators connected to the rotor shaft. One is rated at 65 kW and other is at 13 kW. [40] The system is arranged in such a way that if the wind speed exceeds 8m/s, the larger generator will run and smaller one will operate for the wind speed below 8m/s. This analogy is described in Figure 3.9. In such a topology the larger and the smaller generators rotate at 1212 rpm and 1230 rpm respectively.
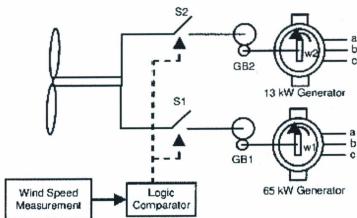

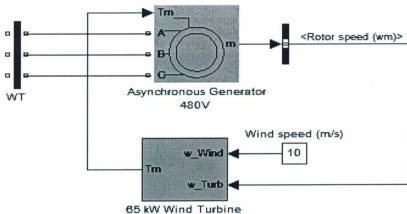Figure 3.9: The 65 kW wind generator and control

Figure 3.10: The 65 kW wind Turbine Model in Simulink

Steady state model of WM15S has been developed here in this section and it is intended to compute that how the energy is being produced with different levels of wind speeds. In the following figure, wind turbine powers for different wind speed have shown for 5 second simulation time.
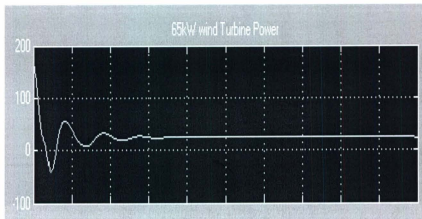

Figure 3.11(a): The 65 kW wind Turbine Power at 6 m/s Wind Speed
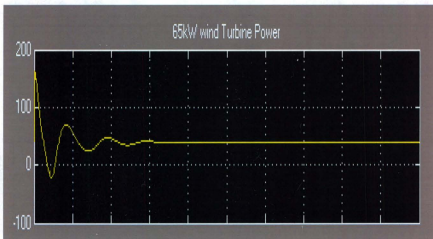
Figure 3.11(b): The 65 kW wind Turbine Power at 8 m/s
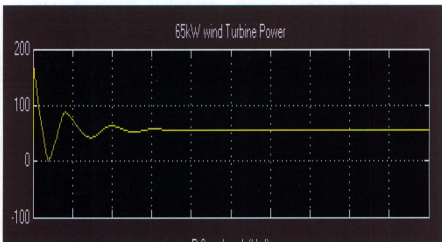Wind Speed

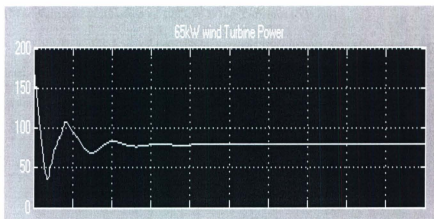Figure 3.11(c): The 65 kW wind Turbine Power at 10 m/s
Wind Speed

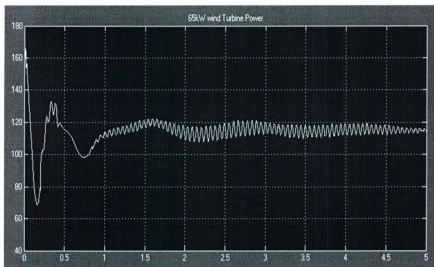Figure 3.11(d): The 65 kW wind Turbine Power at 12 m/s

Wind Speed

Figure 3.11(e): The 65 kW wind Turbine Power at 15 m/s

Wind Speed

Figure 3.13(a): The NW100 Wind Turbine Power at 8 m/s Wind Speed

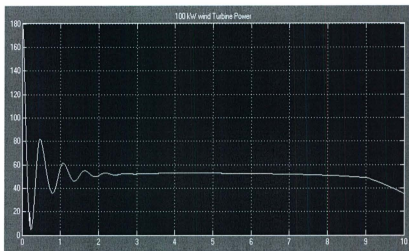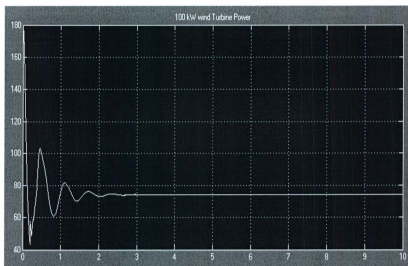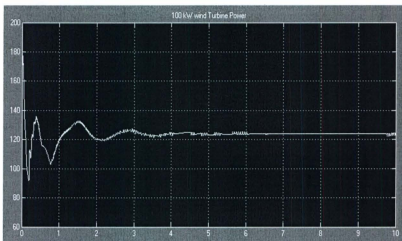Figure 3.13(b): The NW100 Wind Turbine Power at 10 m/s Wind

Figure 3.13(c): The NW100 Wind Turbine Power at 12 m/s Wind Speed
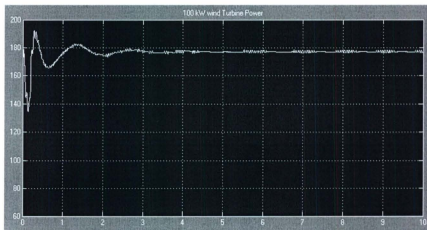

Figure 3.13(d): The NW100 Wind Turbine Power at 15 m/s Wind Speed

Modeling of Diesel Generator

The working principle of diesel generator is explained. Desired and actual speeds are the two inputs to the engine block and the mechanical power is the output from the block

which will further be coupled to the synchronous generator. The engine's characteristics are based on two transfer functions as follows [48],

$$H_c = \frac{(1+T_3.s)K}{(1+T_1.s+T_1T_2.s^2)}$$ .... (3.57)

$$H_a = \frac{(1+T_4.s)}{[s(1+T_5.s).(1+T_6.s)]}$$ .... (3.58)

Where, K is the regulator gain, T_1 T_2 and T_3 are the regulator time constants and T_4, T_5 and T_6 are the actuator time constants. The diesel engine and the excitation parameters are specified in Table 3.2 and 3.3.

Table 3.2 Specifications Diesel Engine

Engine Parameters	Values
Regulator Gain, K	30
Regulator Time Constants (T I, T2, T3	0.0 1,0.02, 0.2
Actuator Time Constants (T4, T5, T6)	0.25,0.009,0.0384
Torque Limit 0- 1.1	0- 1.1
Engine Time Delay, Td	2.4 ms

Table 3.3 Specifications of Excitation System

Engine Excitation Parameters	Values
Low Pass Filter Time Constant	10 ms
Regulator Gain	200
Regulator Time Constant	20 ms
Exciter Gain l	l
Damping Filter Gain	0.1
Damping Filter Time Constant	1.5 s
Regulator Output Limits	0-6 pu

The rated power of diesel generator is 925 kW. Mechanical power and field voltage are the inputs to this generator block and electrical energy according to the demand produced from this block. The SimPower model of the diesel generator associated with the excitation and the engine systems is shown in Figure 3.14 and the generator specifications are presented in Table 3.4.

Parameters	Values	Parameters	Values
Rs	0.0010615 pu	Lkd	4.5675 pu
Ll	0.06 pu	Rkql	0.4939 pu
Lmd	2.86 pu	Lkql	0.548 pu
Lmq	1.98 pu	H	0.6469 s
Rf	0.005759 pu	F	0.005327 pu
F	0.005327 pu	P	2
Lfd	0.0355 pu		

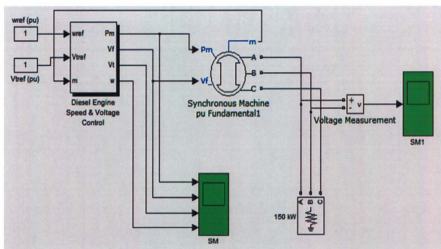Table 3.4 Diesel Generator System Parameters

Figure 3.14(a) Simulink Model of Diesel Generator

The rated power of diesel generator is 925 kW. Mechanical power and field voltage are the inputs to this generator block and electrical energy according to the demand produced from this block. The SimPower model of the diesel generator associated with the excitation and the engine systems is shown in Figure 3.14 and the generator specifications are presented in Table 3.4.

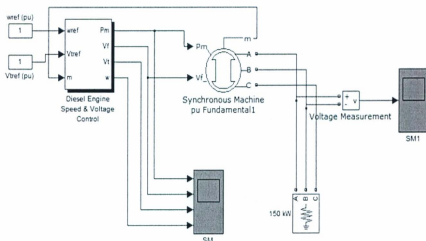| Parameters	Values	Parameters	Values
Rs	0.0010615 pu	Lkd	4.5675 pu
Ll	0.06 pu	Rkql	0.4939 pu
Lmd	2.86 pu	Lkql	0.548 pu
Lmq	1.98 pu	H	0.6469 s
Rf	0.005759 pu	F	0.005327 pu
F	0.005327 pu	P	2
Lfd	0.0355 pu		

Table 3.4 Diesel Generator System Parameters

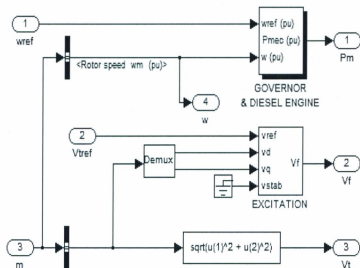Figure 3.14(a) Simulink Model of Diesel Generator

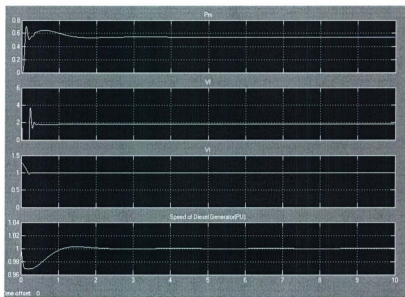Figure 3.14(b) Engine and Excitation System of Diesel Generator

Figure 3.15 Simulation Result of Diesel Generator

3.9 Modeling of Flywheel Storage System

As there is no SimPower system block of Flywheel storage in Simulink, we have the design the flywheel storage system. According to the load characteristics the energy required for sudden variation of wind speed is calculated. The inertia of the flywheel disk was calculated from the mass of the flywheel and from the radius of the wheel for Ramea system. The energy equation of a flywheel storage system can be expressed as follows:

$$E = \frac{1}{2} I. \omega^2 \quad \dots\dots\dots\dots\dots\dots\dots\dots\dots\dots\dots\dots\dots\dots\dots\dots \quad (3.58)$$

Where, I is the moment of inertia in Kg.m^2 and ω is the rotational speed in rad/s.

And also the moment of inertia, I can be expressed as

$$I = \frac{1}{2} MR^2 \quad \dots\dots\dots\dots\dots\dots\dots\dots\dots\dots\dots\dots\dots\dots\dots\dots \quad (3.59)$$

Where, M is the mass of the Flywheel disk, and R is the radius of the Flywheel disk.

The mass of the wheel can be found from the equation as follows:

$$M = \frac{1}{2} \rho \pi h r^2 \dots\dots\dots\dots\dots\dots\dots\dots\dots\dots\dots\dots\dots\dots\dots\dots \quad (3.60)$$

Where, ρ is the density of the material used for the disk, h is the thickness of the flywheel disk and r is the radius of the disk.

Finally the overall energy storage can be stated as :

$$E = \frac{1}{2} MR^2 \omega^2 = \frac{1}{2} (\frac{1}{2} \pi \rho h R^2) R^2 \omega^2 \dots\dots\dots\dots\dots\dots\dots\dots\dots\dots\dots\dots \quad (3.58)$$

For cast steel the density of the material is 7.85 kg/m$^3.$

As calculated in chapter 2 from the system sizing, the minimum amount of back up energy required for Ramea is 25kWhr.

So the required energy E= 25 kWhr, let, the radius of the disk is 1m and the thickness is .05m. If the maximum rotational speed is considered as 7000 rpm the inertia of the machine can be finding as

$$I = \frac{2E}{\omega^2} = \frac{2 * 25 * 1000 * 3600}{7000^2}$$, and I = 3.67 kg.m²

In desired design a permanent magnet synchronous machine as a motor/generator unit. As there is no block of Flywheel storage in Simulink, the calculated inertia was added to the machine inertia in order to make the flywheel model. A phase lock loop (PLL) is used for voltage to frequency conversion. A switching relay is use for the operation of the machine in generating or motoring mode. The principle is that, when the grid frequency goes below 60 Hz then the machine will start discharging. When the grid frequency is exceeds 60 Hz, and then the machine will absorb energy from the grid to maintain a regulated frequency on the grid. The following figures will show the Simulink model of Flywheel storage. For the simulation purpose a step change of load to observe the frequency characteristics of the system is investigated.
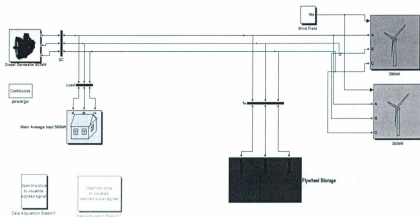
Figure 3.16 Simulink model of Ramea System with Flywheel Storage
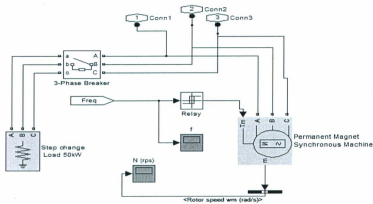
Figure 3.17 Simulink model of Flywheel Storage with Step change in Load
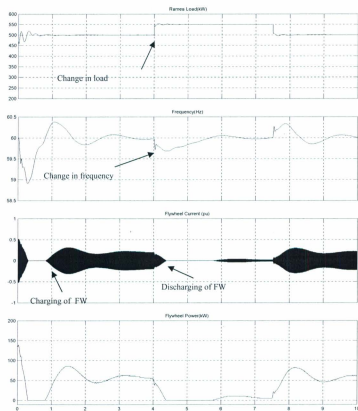
Figure 3.18 Effect of load changing in system frequency and flywheel

charging and discharging characteristics

Figure 3.20 shows that a step change in the load of 50kW will lead to a frequency deviation of 0.3Hz. System flywheel will provide more that 50kW for few seconds to maintain system frequency.

Figure 3.19 Wind turbines and diesel generator simulation output of Ramea hybrid power system from Simulink

3.10 Summary

In this chapter detailed dynamic modeling of wind turbine, diesel generator and FESS and their associated simulation results have been presented and discussed. Asynchronous machine, synchronous machines model with necessary equation have been presented. The transformer models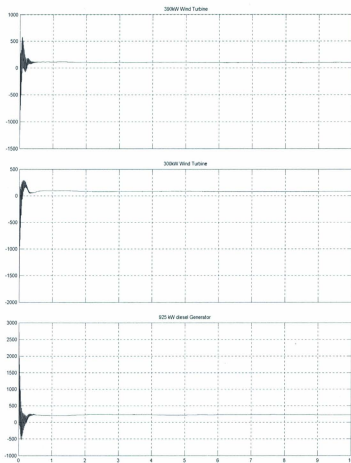 with equivalent circuits have been included in this chapter. The WM15S wind turbine and WM100 wind turbine steady state characteristics have presented for different wind speeds. The diesel characteristics have also shown. Detailed calculation and equation for flywheel storage system is presented. From the dynamic simulation it was found that, the flywheel can deliver energy to the grid when the grid frequency goes below 60 Hz and also can absorb energy from the grid when the grid frequency exceeds 60 Hz. In this way it has been proved that, the proposed flywheel energy storage system is capable of maintaining a stable grid with a regulated frequency. Simulation results have demonstrated that when an increase in the load takes places, system frequency goes down FESS starts discharging. As soon as the load decreases, the system frequency exceeds 60 Hz and FESS starts charging again.

Chapter 4

Experimental Setup and Test Results

The experimental tests are carried out with a DC machine based flywheel energy storage system (FESS). DC machine based FESS technology can be used to provide backup power to an isolated hybrid power system. Flywheels intended for energy back up are typically designed to provide power at their maximum rate for a period of about few second seconds to a few minutes. The objective of the proposed FESS is to minimize the voltage sags or swellings in Ramea hybrid power system. DC machine base FESS can be a good choice for such an application. The use of DC machine makes the storage system simple eliminating one inverter/rectifier unit from the circuit compared to use an AC (Alternating Current) machine based system.

4.1 DC Machine-Based Flywheel Energy Storage System

A dc machine based FESS consist of a dc motor/generator unit coupled with a flywheel disk, a controllable power supply unit with control input voltage(dc), a main control unit, a dc-dc converter, an inverter and its protection circuit. There is also a field control power supply present in the system to control the field of the dc machine.
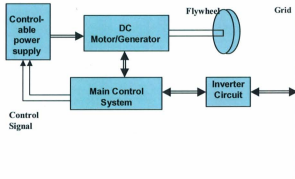
Fig.4.1 DC System Flywheel Storage

DC system flywheel energy storage technology can be used as a substitute for batteries to provide backup power to an uninterruptible power supply (UPS) system. Although the initial cost will usually be higher, flywheels offer a much longer life, reduced maintenance, a smaller footprint, and better reliability compared to a battery. The combination of these characteristics will generally result in a lower life-cycle cost for a flywheel compared to batteries.

Flywheels intended for UPS application are typically designed to provide power at their maximum rate for a period of about 15 seconds. In contrast, most

batteries for UPS applications are designed to provide their maximum-rated power for about 15 minutes. Therefore, using a fly-wheel instead of batteries will generally require a generator that can come up to full power within about 10 seconds, which is well within the capabilities of stand-by generators.

In the upcoming section of this chapter each, component used in this experimental setup are described. Different charging and discharging characteristic have been shown. Three different loads have been applied to observe the generator terminal voltage characteristics. The efficiency of the machine for each case was found from the input and output measured powers. Depending upon the characteristic curves, parameters for optimum energy storage have been determined. These parameters are very important for designing the control system. The experimental set-up with the proposed control system design consists of the following components:

   i. Controllable power supply (two)

   ii. Phase control relay, 6V dc (two)

   iii. Electromechanical relay(two)

   iv. DC machine (3Hp/2kw, 1750RPM, 120V)

   v. Data acquisition card [MCC1208LS] from measurement computing.(one)

      vi. Voltage and Current Sensor (one)

      vii. Speed Sensor [output 0-10V dc](one)

      vii. Cast steel Flywheel rotor (one)

      viii. Logic Power Supply(+/- 15 Volts, DC)

      ix. A personal Compute
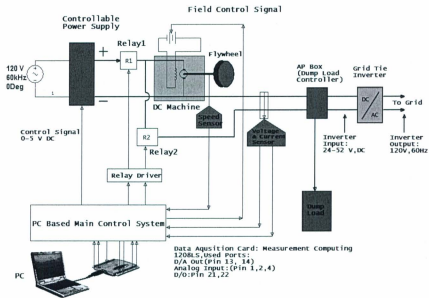
Fig:Schematic Diagram of Flywheel Energy Storage

Fig.4.2 Control Block Diagram of Flywheel Storage

4.2 DC Current Transducer (CR5200)

In our experimental set-up, two CR5200 Series DC current transducer are used to sense the input and output current of the DC machine. DC Current Transducers are designed to provide a DC signal which is proportional to a DC sensed current. These devices are designed for direct current only, targeting them towards general and daily applications. The ranges 2 to 10 Amps utilize an advanced Magnetic Modulator technology and the ranges 20 amps and above utilize Hall Effect technology.

Fig. 4.3 Current Transducer

SPECIFICATIONS

Basic Accuracy:	1.0 %	Output Load: ±5 or ±10 VDC	2 K Ω or greater
Thermal Drift:	500 PPM/°C	4-20 mADC	0 - 300 Ω
Operating Temperature:	0°C to +50°C	Supply Current:	
Response Time:	250 ms. max.,0-90%	CR5210:	Typical 35mA Max 40mA
FS		CR5210S:	Typical 30mA Max 35mA
Insulation Voltage:	2500 VDC	CR5220:	Typical 60mA Max 100mA
Supply Voltage:	24 VDC ±10%	CR5220S:	Typical 40mA Max 50mA
Frequency Range:	DC only	Torque Specs:	3.0 inch lbs. (0.4Nm)
MTBF:	Greater than 100 K hours	Weight:	0.5 lbs.

4.3 Calibration Equation for the Current Sensor:

A current sensor is used to sense the motor armature current, which is to calculate the total power of the energy storage system. Varying the current through the current sensor, the output voltages are recorded. A statistical model is also developed by obtaining the calibration equation. The calibration equation is as follows:

$Va = 2.035 x Ia - .0548$
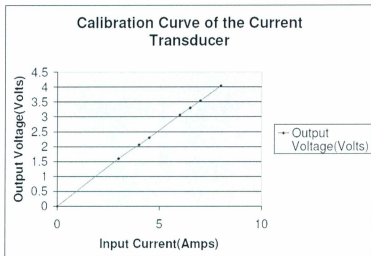
Fig. 4.4 Transducer Current vs Voltage

4.4 Amplifier Circuit:

A double gain amplifier circuit was necessary for the system. Because the output from the microcontroller is in the range from 0 to 5 volts while the control signal to the input of the phase control relay is about 0 to 10 volts. As a result two double gain amplifier circuits are required for out experimental set-up. LM741 IC is used as a non inverting amplifier and +/- 15 volts are used for biasing the operational amplifier.
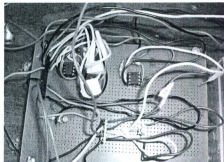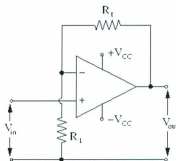
Fig. 4.5 Double gain amplifier Circuit

4.5 Calibration Equation for the Rotational Speed of the DC Motor

A tacho generator was attached to the motor shaft to generate a voltage corresponding

to the rotational speed of the motor. The output voltage of the tacho generator was

between 0 to 10 volts. Several voltages were applied to the motor armature and the

tacho generator voltages were recorded.
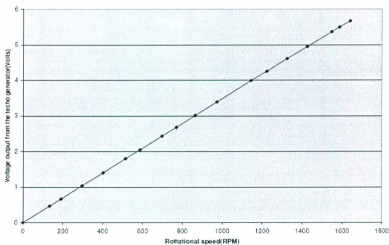
Fig 4.6 Calibration Curve for the Rotational Speed of the Motor

The armature voltage was increased using computer to avoid error. A model for rotational speed vs. tacho output was calculated and the curve generated by the model is presented in figure 4.4. The resulting calibration equation was

$$W_m = 288.51*V - 3.3896 \quad \cdots\cdots\cdots\cdots\cdots\cdots\cdots\cdots\cdots\cdots\cdots\cdots\cdots\cdots\cdots\cdots\cdots (4.1)$$

4.6 Voltage Sensor

For the purpose of power measurement, we need to measure voltage and current both. The current was measured by current transducer and the voltage was measured by two voltage isolators. The voltage isolator was used because of the recording the value in PC through the data acquisition card. It should be mentioned that, the data acquisition card only can read voltage between 0 to 10 volts.
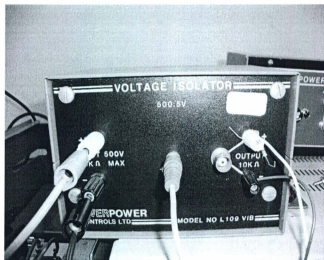
Fig 4.7 Voltage Sensor

4.7 Logic Power Supply Unit:

Two logic power supply unit are used for the laboratory set-up. The logic power supply units are necessary to power the voltage isolator and the amplifier circuit. Output of the logic power supply are -/+ 15 volts. This logic power supply is required for the op-amp amplifier circuit.

Fig 4.8 Logic Power Supply

4.8 Calibration Equation of the input and the output of the controllable power supply unit:

The output of the controller is applied to the control input of the controllable power supply unit. The phase control relay of the power supply unit can accept only voltage ranging from 0 to 10 volts DC. Due to possible non linearities in the relay , a calibration equation is derived to reflect the actual controller voltage and the relay input voltage.
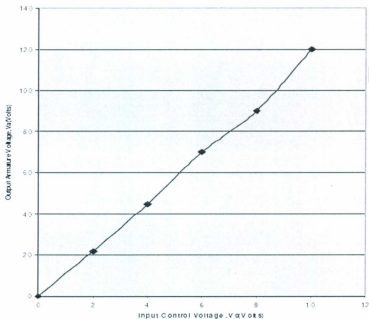
Fig 4.9 Calibration Curve for the Controllable Power Supply Unit

The calibration curve is by changing the dc voltage from 0 to 10 volts to the input of the phase control relay, and observing the output of the power supply unit. From the calibration curve a calibration equation is found as:

$$Va = .0022 * Vc^2 + .201 * Vc - 0.56 \quad \dots\dots\dots\dots\dots\dots\dots\dots\dots\dots\dots\dots\dots\dots(4.2)$$

4.9 DC Machine Parameter Calculation

The separately excited DC motor used in experimental testing is rated at 3 HP while working as a motor and 2 kW while working as a generator. In the both cases the terminal voltage is 125 volts DC, with a full load current of 16 Amps. The parameters of the machine are determined through experimentation rather than assuming the value provided by the manufacturer. The following procedures are used to obtain the parameters.

4.9.1 Armature Resistance

The armature resistance of the motor was determined by applying a DC voltage at the armature terminal and measuring the corresponding current. The experimental recorded values are shown in Fig. 4. 10. In order to reduce the error on the armature resistance, several readings were taken and a mean value was taken which was 0.4 ohm.

determination of Ra
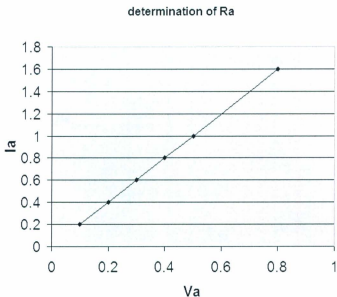
Fig. 4.10 Experimental curve to determine armature resistance

4.9.2 Inertia

Several methods exist to determine the inertia of a dc drive. A review of the existing method by Lin [69] found that most methods lead to uncertainty in the parameters. In this purpose a general approach was considered which is based on the following equation [69]:

$$Jm = \frac{T_m * K_t * k_e}{Ra}$$ .... (4.3)

Where,

J_m is the moment of inertia of the motor,

T_m is the mechanical time constant of the motor,

K_t is the torque co-efficient of the motor and

R_a is the armature resistance of the motor.
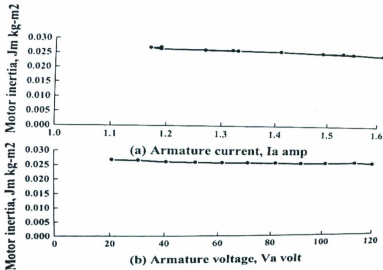
Fig. 4.11 Variation of the motor inertia with, (a) armature current, (b) armature voltage

The mechanical time constant of the motor was determined by rotating the motor to its base speed and then shut down the power and recording the time it taken to reach 36.3% of its base speed. [69]. It was found that the inertia of the motor was almost constant regardless of the variations in the motor armature voltage or current. A mean value was used to minimize the error and the inertia of the motor was 0.026042 kg-m^2.

the variation of the motor inertia with respect to the armature current and voltage are shown in Fig. 4.11(a) and 4.11(b) respectively.

4.9.3 Back Emf Constant

The back emf constant was found as follows [69]

$$k_e = \frac{v_{noload}}{w_{noload}}$$ .... (4.3)

Where, v_{noload} is the no load voltage of the armature and w_{noload} is the no load speed of the motor [61]. It can be found that the back emf constant is more or less constant regardless the variation of armature voltage or current. The back emf constant of the motor was found to be 73.167 v/krpm. The experimental back emf constant with the variation of armature current and voltage are shown in figure 4.11(a) and 4.12(b) respectively.

Fig. 4.12 Variation of the motor back emf constant with,

(a) armature current, (b) armature voltage

4.9.4 Torque Co-efficient

The torque co-efficient was calculated as described below [69]

$$k_t = 9.5439e - 3 * k_e \quad .... \quad (4.4)$$

Where, K_e is the back emf constant in V/krpm.

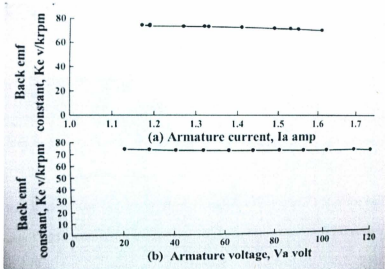The experimental torque coefficient with the variation of armature current and voltage are presented in Figure 4.13(a) and 4.13 (b) respectively. The value of the torque coefficient was found as 0.0711 kg.m/A.
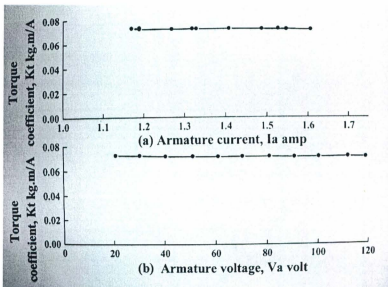

Fig. 4.13 Variation of the motor torque constant with, (a) armature current, (b) armature voltage

In order to reduce the error, several readings have been taken for emf constant and the torque coefficient, and a mean value was taken.

4.10 Flywheel (Inertia Disk)

The inertia of the wheel is a critical part of the research. It largely depends on the rotor radius, blade length and material. The inertia disk was designed using the following approach.

For a solid cylinder, the inertia is given by [70]

$$J_w = 1/2 * M * (R_{disk})^2 \ldots\ldots\ldots\ldots\ldots\ldots\ldots\ldots\ldots\ldots\ldots\ldots\ldots\ldots\ldots\ldots\ldots (4.5)$$

Where, M is the mass of the solid disk and R_{disk} is the radius of the disk.

Mass, M = Volume * Density.

Cast steel C10/C20 was considered for the disk. From (4.5) the thickness was calculated by choosing suitable radius and it was found that the disk is around 46 kg adequately can handle a 2 kW DC generator.

4.11 Electromechanical Relays

Electromagnetic relays generally comprise two primary components including a movable conductive cantilever beam and an electromagnetic coil. These relays have one or more mechanical displacement electrical contacts coupled to a mobile element of the magnetic circuit of an electromagnet. The electromagnet is controlled by supplying power to its coil which drives the movement of the mobile element and the closing or opening of the electrical contacts of the relay. Electromechanical relays are used in various applications, such as instrumentation, telecommunications, automatic test systems, wireless technologies, RF signal pulse generators, automotive and

medical electronics, as well as commercial and general aviation and aerospace applications.
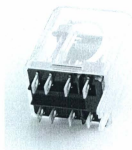
Fig. 4.14 Electromechanical Relay

In our experimental set-up two 120/240 V AC relays are employed. These relays can handlemaximum current of 10Ams and it can be operated by a 5 volt DC signal. The relay is used to connect and disconnect the generator to the load and the main supply. Relay driving circuit was necessary for the smooth operation of the relays.

4.12 Relay Driving Circuit

The driver circuits are simply based on PNP transistor where transistors are working as switches. The transistors are activated by the control signal (logic 0-5V) coming

from the system controller. Resistors are used to limit the voltage applied across the relay coil.

Relay Driving Circuit:
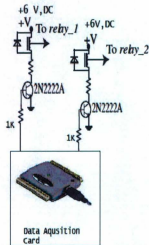
Deatails of the Drive Circuit:

Relay:1/4 HP,120V AC,240V AC
Part No:KUPILD55
Coil:6V DC, 10A
Manufacturer:Potter & Brumfield

Transistor:
NPN, 2N2222A
VCC=+10V DC

Data Aquisition Card:
Company:Measurement Computing
Part No: USB1208LS
Used Ports: AO(Pin-21) and A1(pin-22)

Fig. 4.15 Relay Driving Circuit

4.13 Data Acquisition Card

In this experiment a data acquisition card (USB-1208LS from Measurement Computing) is used for data acquisition and control purposes. The Data acquisition card can be programmed either in Visual Basic or C++ language. The Visual Basic language was used for the experiment. The USB-1208LS from Measurement Computing is a low speed USB device that features 8 analog inputs, 2 10-bit analog

outputs, 16 digital I/O connections, and 1 32-bit external event counter. The USB-1208LS analog inputs are software configurable for either 8 11-bit single-ended inputs, or 4 12-bit differential inputs. An on-board industry standard 82C55 programmable peripheral interface chip provides the 16 digital I/O lines in 2 8-bit ports. Each digital port can be configured independently for either input or output. The USB-1208LS is powered by the USB port on a personal computer (PC). No external power is required.

Fig. 4.16 Data Acquisition Card

4.14 Experimental Setup

A PC control based flywheel energy storage system (FESS) is designed, tested and verified in the energy system lab of Memorial University of Newfoundland. The data acquisition card interfaced with the PC is the key controlling device for the system. Phase control relays are used to control the armature and the field of the dc machine. Electromechanical relays are used to connect or disconnect the load and the supply according to the control signal comes from the data acquisition card. Speed sensor is

used to monitor the flywheel rotation. Voltage and current sensor are use to find out the amount of energy flow and to maintain a stable grid providing the signals to the main control unit. The experimental set up is shown in the figure 4.16 and 4.17.
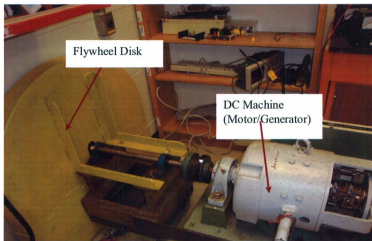
Fig. 4.17 Experimental set-up of a DC machine based Flywheel Energy Storage System
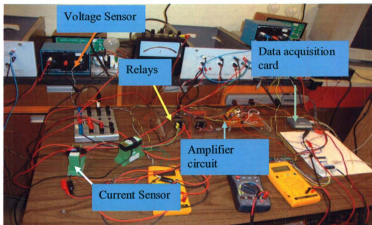
Fig. 4.18 Experimental set-up of a DC machine based Flywheel Energy Storage System with various components
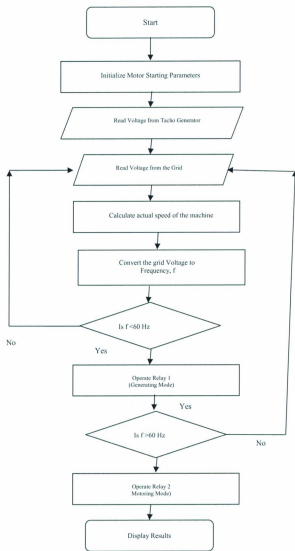
Fig. 4.19 Control Flowchart of Flywheel Storage System

4.15 Test Results

In this experiment, different readings are recorded to determine a best control strategy for the energy flow of the FESS. The DC motor armature was supplied by different voltage level and the amounts of energy required for each time are calculated. Basically the tests are carried out with different armature voltages, different speed limits and different field voltages while in charging mode. On the other hand, different loads and different field voltage are applied to the generator terminal while in discharging mode. Various test results are shown in the following figures: (define sample time. X-axis labels are missing below)
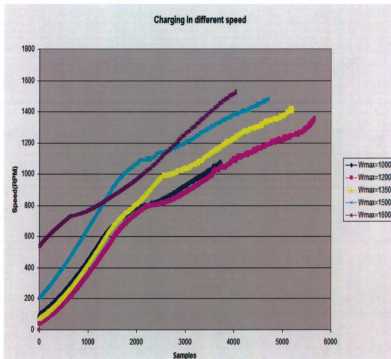
Fig. 4.20 Experimental curves while charging in different speed
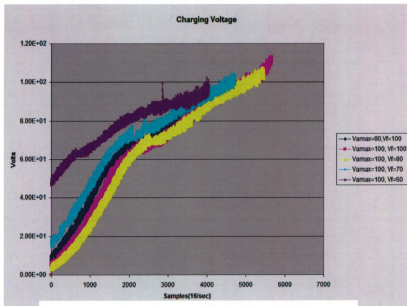
Fig. 4.21 Experimental curves while charging with different

maximum armature and field voltage
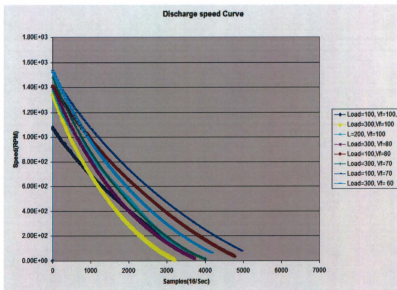
Fig. 4.22 Speed variations with different load and different field

voltage while in discharging mode.
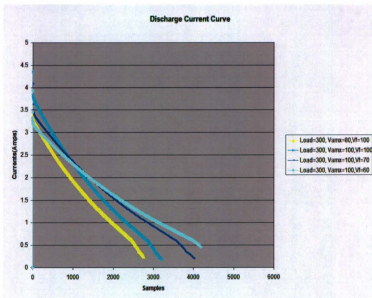
Fig. 4.23 Current variations with different load and different field
voltage while in discharging mode.
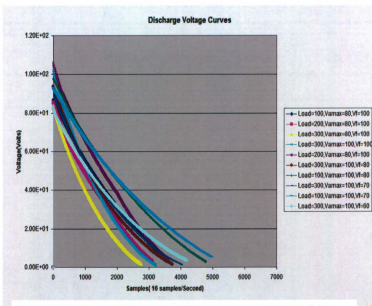
Fig. 4.24 Current variations with different load and different field
voltage while in discharging mode.
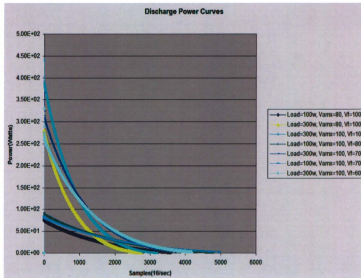
Fig. 4.25 Power variations with different load and different field

voltage while in discharging mode.

From the above test results, the efficiency of the DC generator was determined for

each and every case. The summary of observations have shown in Table-II

Table-II
Summary of Observations

Armature Voltage V_{amax} (Volts)	Field Voltage V_f(Volt)	Load(W)	Charge Energy (?)	Discharge Energy(?)	Efficiency (%)	Chrage Time (Sec)	Discharge Time (Sec)
80	100	100	1.85E+01	1.04E+01	56.21621622	235	223
80	100	200	1.84E+01	1.03E+01	55.97826087	264	194
100	100	200	3.06E+01	1.74E+01	56.92810458	340	225
100	80	100	3.33E+01	1.81E+01	54.34913017	341	300
80	100	300	1.88E+01	1.02E+01	54.25531915	235	172
100	100	300	3.24E+01	1.71E+01	52.87037037	353	201
100	80	300	3.34E+01	1.69E+01	50.5988024	325	233
100	70	300	3.54E+01	1.95E+01	55.08474576	295	250
100	70	100	3.57E+01	1.82E+01	50.98039216	356	309
100	60	300	3.12E+01	1.73E+01	55.44871795	353	231

From Table-II one can see that, maximum period of charging is 353sec with armature voltage of 100 volts and field voltage of 100 volts. The minimum time taken for charge the DC motor is 235 seconds with armature and field voltage of 80 volts and 100 volts respectively. The maximum time to discharge while in generating mode of the DC machine is 309s with a field voltage of 70V and with 100 watts bulb load. The minimum time taken to discharge the generator is 172 seconds with a load of 300 watts bulb and with a field voltage of 100 volts. The efficiency of the machine was calculated for each condition and is found ranging between 50% to 57 %. The above summary and readings are very important for designing the proper control strategy of the DC FESS. In the following section the details of control strategy are described.

4.16 Control Parameters and Design of Control System

Based upon the test results from the previous section, the control parameters can be selected for the minimum charging time and maximum discharging period. The objective is to find out the condition for minimum charging energy and also the conditions for maximum discharge energy. These parameters are found as follows:

❖ Minimum Charging Parameters
   -Vamax=80 Volts, V_f = 100 Volts

❖ Maximum Discharging Parameters
   -V_f= 100, Load= 100 Watts

With the above parameters, the control strategy is determined. A PC based control system is developed for the system in order to charge and discharge FESS. The armature voltage was controlled through the analog output of the data acquisition card. The control signal is sent to the control input of the controllable power supply unit.

There is an amplifier circuit used in between the data acquisition and the input of the power supply unit because the output of the data acquisition card is in the range of 0 to 5 volts. This voltage has to be increased up to 10 volts to utilize the full range output voltage of the controllable power supply unit. The electromechanical relays are controlled by the digital signal of the data acquisition card, wher the control point is set inside the Visual Basic program for connection and disconnection of the electromechanical relays. The following Figure shows the diagram of armature control system.
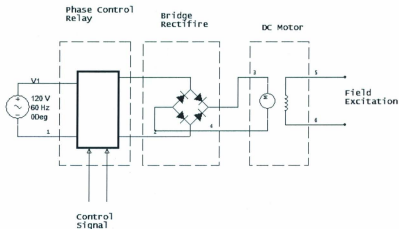
Fig 4.26 Armature Control Circuit

The controllable power supply unit consists of a phase control relay and a bridge rectifier. The control signal is send to the control input of the phase control relay, the output of the bridge rectifier is connected to the armature of the DC machine.

Electromechanical relays are used in between the power supply unit and the armature of the DC machine.

Fig: Field Excitation Control of a DC Machine
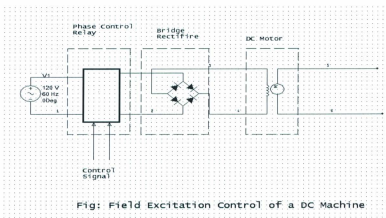
Fig 4.27 Field Excitation Control Circuit

The field control circuit is necessary for keeping the field excitation in different levels over different time intervals. The strategy is same as the armature control circuit and the second analog output of the data acquisition card is used for this purpose.

In Fig 4.27 a detailed control schematic is shown. In this experimental tests, resistive loads are used to verify the ability of the FESS to deliver energy to the load. The test results show that the DC machine based FESS can deliver power to the load instantly as a source energy backup. The duration of the energy delivery depends on the design of the system and also the size of the flywheel. This is basically a predefined on /off type control system designed for the DC machine-based FESS. The whole idea is that,

when the grid frequency drops lower than 60 Hz the output of frequency to voltage converter also goes down. The sensor senses the frequency change and generates a control signal which is used to control the DC machine. In a similar way, when the grid frequency is higher then, a motoring control signal is sent to the DC machine to absorb energy from the grid. In this way the voltage and frequency regulation are achieved with the DC machine based FESS.

4.17 Summary

In this chapter, a brief description of various components used in the experiment has been given. Various DC motor parameters have been shown including armature voltage, speed, current and power characteristics. System calibration curves have been provided where, calibration curves are utilized for retrieving actual values of voltages, currents and the rotational speeds of the DC machine. Test results have been presented with a number of armature voltages, field voltages and with different rotational speeds while in charging mode. In discharging mode, characteristics have been shown with a number of load and different field excitation. The efficiency of the generator for the each case has been determined. A control strategy based on experimental test results has been stated. From the charging and discharging readings, the maximum generating energy and the minimum charging energy have been determined to design the optimum control system. The whole control strategy has been designed, tested and verified in the Energy System Lab of Memorial University of Newfoundland.

Chapter 5

5.1 Conclusions

In this research, we proposed a flywheel energy storage system (FESS) to the existing Ramea hybrid power system. The system basically includes a two way energy flow scheme so that energy is injected into the flywheel in the form of kinetic energy, and drawn from the machine driving the flywheel in the form of electric energy. After showing the block diagram for our system and providing some general system description, we have presented the system sizing and steady state simulation which is done using Homer software. Various comparative results of steady state simulation are presented with and without flywheel energy storage system for Ramea Hybrid power system. The usefulness of the proposed Flywheel Energy Storage system has been discussed, and the components of the hybrid power system were described briefly. From the Homer simulation it is clear that, addition of single flywheel storage to the current power system of Ramea will be very effective. It will reduces the fossil fuel cost per year, excess energy will be less, number of starts of the generators will be reduced and thus life time of the generator will increase to a great extent. Different hazardous gases like CO_2 and SO_2 emission will be decreased which is one of the most important environmental issues. System is also modeled using SIMULINK, and simulated to study dynamics. System dynamics characteristic have been shown. The simulation results were

very close to the anticipated ones, and we can see that flywheel can deliver and draw energy when it is necessary to maintain a regulated grid frequency. After finishing steady state and dynamic simulation of the hybrid power system an experimental setup to design, test and to verify a suitable control method for the proposed Flywheel Energy Storage System for Ramea hybrid Power System is developed in the lab. Experimental results have been shown and the parameters for designing optimal control strategy are presented. It should be noted that, the designed control system with the DC machine have been tested and verified in the energy system lab of Memorial University. The result shows that flywheel can effectively deliver energy to the load and also can take power as a load while in motoring mode. Various aspects that affect the FESS including economical, environmental were taken into consideration.

5.2 Future Work

As the wind energy is a clean source of energy so it is expected that, maximum power from the wind will be used for the remote community of Ramea. Here in our research we proposed flywheel storage for short term energy back up. But for utilizing the maximum benefit from the wind energy, long term storage could be a good choice. NL hydro already decided to introduce hydrogen storage on the site. But the problem is that, it has very low efficiency. Pump hydro could be a good solution to overcome the efficiency problem. In September, 2009 we visited Ramea to view the existing hybrid system of the island. From the site survey it was found that, there is a suitable place for pump hydro installation. Pump hydro needs few seconds for coming online with full capacity. Flywheel storage can be use intermittently for this purpose also.

On the other hand, advanced flywheels can be introduced in order to increase the system efficiency. Advanced flywheel system rotate above 20,000 rpm in vacuum enclosure made from high strength carbon composite filament will be very efficient. In high speed applications, magnetic bearings will reduce the friction losses and can have efficiency as high as 80%. Focus should be on increasing the speed of the flywheel rather than the moment of inertia because its kinetic energy increases geometrically with speed.

5.3 List of Publications:

1. K.Islam, M.T. Iqbal "Flywheel Energy Storage System for an Isolated Wind-Hydrogen-Diesel Power System" Presented in WESNet Poster Presentation, CanWEA, 2010, Montreal, Canada

2. K.Islam, M.T. Iqbal and R. Ashshan "Sizing and Simulation of Flywheel Energy Storage System for Ramea Hybrid Power System" Presented at 19th IEEE-NECEC Conference 2010, St. John's, Canada

3. K.Islam, M.T. Iqbal and R. Ahshan "Experimental Observations for Designing & Controlling of Flywheel Energy Storage System" Presented at 19th IEEE-NECEC Conference 2010, St.John's, NL, Canada

4. K.Islam and M.T Iqbal "Sizing and Control of Flywheel Energy Storage for a Remote Hybrid Power System" Presented at WESNet Workshop, February 24-25, Ryerson University, Toronto, ON, Canada 2011.

Appendix A
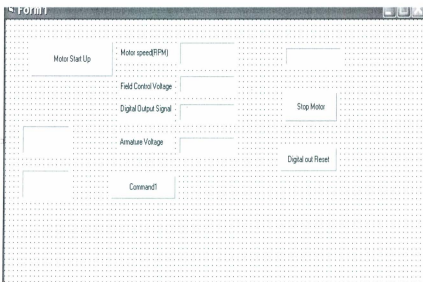
Figure 5.1: Visual Basic Environment for Control of Flywheel Energy Storage

Visual Basic Code:

```
'***** Visual Basic Code for Control of Flywheel Energy Storage *******

Private Declare Sub Sleep Lib "kernel32" (ByVal dwMilliseconds As Long)

Private Sub Analog_Read_Click()
'************8 Armature Control****************************************
Dim j As Single
Dim k As Single
Dim u As Double
v1 = 5
Gain = UNI5VOLTS    ' set the gain
Chan% = 1 'output channel
```

```
Const Range% = UNI5VOLTS
AO_data = Val(v1) 'Data range 0-4095
Picture6.Cls
Picture6.Print v1
DataValue% = (v1 / 5) * 1023
ULStat% = cbFromEngUnits(0, Range%, AO_data, DataValue%)
If ULStat% <> 0 Then Stop
ULStat% = cbAOut(0, Chan%, Range%, DataValue%)
If ULStat% <> 0 Then Stop


For j = 1 To 1350
v = 1 + (j / 350)
  'For k = 1 To 5000000
  'Next k
Picture3.Cls
Picture3.Print v
Chan% = 0 ' output channel
'Const Range% = UNI5VOLTS
AO_data = Val(v) 'Data range 0-4095
DataValue% = (v / 5) * 1023
ULStat% = cbFromEngUnits(0, Range%, AO_data, DataValue%)
If ULStat% <> 0 Then Stop
ULStat% = cbAOut(0, Chan%, Range%, DataValue%)
If ULStat% <> 0 Then Stop
Sleep 250
Next j

u = (DataValue * 5 / 1023)
Label1.Caption = Format$(u, "0.00")

'*************** end of Armature Control***************************


 ' Collect the data with cbAIn%()

   ' Parameters:
   '   BoardNum%   :the number used by CB.CFG to describe this board
   '   Chan%       :the input channel number
   '   Gain        :the gain for the board.
   '   DataValue%  :the name for the value collected


   Gain = BIP10VOLTS          ' set the gain
   Chan% = 0  ' set input channel
```

```
  ULStat% = cbAIn(BoardNum%, Chan%, Gain, DataValue%)
  vi = (20 * (DataValue% / 4095) - 10)
  'Label2.Caption = Format$(vi, "0.00")
  speed = (288.51 * vi) - 3.3896
  Picture2.Cls
  Picture2.Print speed
  If vi > 2 Then
 Const PortNum% = FIRSTPORTA    ' use auxlary digital port
Direction% = DIGITALOUT  ' program first digital port for output mode
ULStat% = cbDConfigPort(0, PortNum%, Direction%)
11 DO_data = Val(1)
Picture4.Cls
Picture4.Print DO_data
ULStat1% = cbDBitOut(0, PortNum%, 0, DO_data)

'**********************************************
Chan% = 0 ' output channel
'Const Range% = UNI5VOLTS
AO_data = Val(0) 'Data range 0-4095
DataValue% = (0 / 5) * 1023
ULStat% = cbFromEngUnits(0, Range%, AO_data, DataValue%)
If ULStat% <> 0 Then Stop
ULStat% = cbAOut(0, Chan%, Range%, DataValue%)
'**********************************************
"" ****************** Field
Control*************************************************


  'Chan% = 1 ' set input channel
  'ULStat% = cbAIn(BoardNum%, Chan%, Gain, DataValue%)
  ' Va = (20 * (DataValue% / 4095) - 10)
  'If Va > 5 Or Va < 2 Then
   'If Va < 2 Then
   ' Vc = 4
   ' Chan% = 1 ' output channel
   ' Const Range% = UNI5VOLTS
   ' AO_data = Val(Vc) 'Data range 0-4095
   ' DataValue% = (Vc / 5) * 1023
   'ULStat% = cbFromEngUnits(0, Range%, AO_data, DataValue%)

   ' Else
   ' Vc = 2.5
   ' Chan% = 1 ' output channel
   'Const Range% = UNI5VOLTS
   'AO_data = Val(Vc) 'Data range 0-4095
```

```
    'DataValue% = (Vc / 5) * 1023
    ' ULStat% = cbFromEngUnits(0, Range%, AO_data, DataValue%)
    ' End If

   'Else
   'Vc = Vc
   'Chan% = 1 ' output channel
   'Const Range% = UNI5VOLTS
   'AO_data = Val(Vc) 'data range 0-4095
   'DataValue% = (Vc / 5) * 1023
   ' ULStat% = cbFromEngUnits(0, Range%, AO_data, DataValue%)

  'End If
Else
 Direction% = DIGITALOUT   ' program first digital port for output mode
 ULStat% = cbDConfigPort(0, PortNum%, Direction%)
10 DO_data1 = Val(0)
Picture1.Cls
Picture1.Print DO_data1
ULStat1% = cbDBitOut(0, PortNum%, 0, DO_data1)
End If

 ' Gain = BIP10VOLTS          ' set the gain
 " Chan% = 0 ' set input channel
 ' ULStat1% = cbAIn(BoardNum%, Chan%, Gain, DataValue1%)
 ' Vi1 = (20 * (DataValue1% / 4095) - 10)
 "If Vi1 < 4 And Vi1 > 3.8 Then
 ' If Vi1 < 4 Then
 '  GoTo 10
 '  Else
 '  GoTo 11
 '  End If
"
*******************************************************************
******************************

  If ULStat1% = 30 Then MsgBox "Change the Gain argument to one supported by this
board.", 0, "Unsupported Gain"
  If ULStat1% <> 0 Then Stop

  ULStat1% = cbToEngUnits(BoardNum%, Gain, DataValue1%, EngUnits!)
  If ULStat1% <> 0 Then Stop
```

```
'lblShowData.Caption = Format$(DataValue%, "0")   ' print the counts
'lblShowVolts.Caption = Format$(EngUnits!, "0.000") + " Volts"   ' print the voltage

End Sub

Private Sub Command1_Click()
Dim current As Single
Dim speed As Single
Dim t1 As Single
Dim t0 As Single

t0 = 0.03995
t1 = 0
Open "filesSpeed" For Output As #2
Open "filesCurrent" For Output As #3
Gain BIP10VOLTS
Chan% = 3
ULStat% = cbAIn(BoardNum%, Chan%, Gain, DataValue%)
vi = ((20 * DataValue% / 4095) - 10)
speed = (288.51 * vi) - 3.3896
Gain BIP10VOLTS
Chan% = 2
ULStat% = cbAIn(BoardNum%, Chan%, Gain, DataValue%)
current = ((20 * DataValue% / 4095) - 10)
t1 = t1 + t0
Write #3, speed, t1
Write #2, current, t1

End Sub

Private Sub Command2_Click()
Const PortNum% = FIRSTPORTA   ' use auxlary digital port/use port A as digital port
Direction% = DIGITALOUT   ' program first digital port for output mode
ULStat% = cbDConfigPort(0, PortNum%, Direction%)
DO_data = Val(0)


ULStat% = cbDBitOut(0, PortNum%, 0, DO_data)
End Sub

Private Sub Stop_Click()
Chan% = 0 ' output channel
Const Range% = UNI5VOLTS
AO_data = Val(0) 'Data range 0-4095
DataValue% = (v / 5) * 1023
```

```
ULStat% = cbFromEngUnits(0, Range%, AO_data, DataValue%)
If ULStat% <> 0 Then Stop
ULStat% = cbAOut(0, Chan%, Range%, DataValue%)

Chan% = 1 ' output channel
'Const Range% = UNI5VOLTS
AO_data = Val(0) 'Data range 0-4095
DataValue% = (v / 5) * 1023
ULStat% = cbFromEngUnits(0, Range%, AO_data, DataValue%)
If ULStat% <> 0 Then Stop
ULStat% = cbAOut(0, Chan%, Range%, DataValue%)


End Sub
```

References:

[1] R. Hebner, J. Beno, A. Walls, "Flywheel batteries come around again", IEEE Spectrum, April 2002, pp. 46-51.

[2]. W. H. Kim, J. S. Kim, J. W. Baek, H. J. Ryoo, G. H. Rim, Improving Efficiency of Flywheel Energy Storage System with A New System Configuration; Sung-Ju Dong, Chang-Won, Kyung-Nam, Korea ;Korea Electrotechnology Research Institute; Korea Institute of Machinery & Metals.

[3]. Weissbach, R.; Karady, G.; Farmer, R.; A Combined Uninterruptible Power Supply and Dynamic Voltage Compensator Using a Flywheel Energy Storage System; IEEE Transactions on Power Delivery, Vol. 16, No. 2; April 2001

[4]. Alan, I.; Lipo, J.; "Induction Machine Based Flywheel Energy Storage System"; IEEE Transactions on Aerospace and Electronic Systems; Vol. 39, No. 1; January 2003

[5]. Bomemann, H.; Sander, M.; "Conceptual System Design of a 5 MWh/100 MW Superconducting Flywheel Energy Storage Plant for Power Utility Applications"; IEEE Transactions on applied superconductivity; vol. 7, NO. 2, June 1997

[6]. Boyes, J.; Clark, N.; "Technology for energy storage flywheels and super conducting magnetic energy storage"; Proceedings of the IEEE Power Engineering Society Transmission and Distribution conference; V. 3, 2000

[7]. Fang, J.; Lin, L.; Yan, L.; Xiao, L.; "A New Flywheel Energy Storage System Using Hybrid Superconducting Magnetic Bearings"; IEEE Transactions on applied superconductivity; Vol. 1 I, No. I, March 2001

[8]. Leclercq, L.; Robyns,B.; Grave, J.; "Control based on fuzzy logic of a flywheel energy storage system associated with wind and diesel generators"; Elsevier Database; retrieved via www.elsevier.com ; 2003

[9]. Swett, D.; Blanche, J.; "Flywheel Charging Module for Energy Storage Used in Electromagnetic Aircraft Launch System"; IEEE Transactions on Magnetics; Vol. 41, No. 1; January 2005

[10] T. Siostrzonek, S. Piróg, "The Flywheel Energy Storage with Brushless DC Motor - the Practical Results", EPE-PEMC 2006 – September 2006, Portoroz, Slovenia.

[11] B. Wang, G. Venkataramanan, "Dynamic Voltage Restorer Utilizing a Matrix Converter and Flywheel Energy Storage", Industry Applications Conference, 2007. 42nd IAS Annual Meeting. Conference Record of the 2007 IEEE, Volume, Issue , 23-27 Sept. 2007 Page(s):208–215.

[12] J. Silva, B. Borges,. Anunciada, "Improving Control Strategies for HF Resonant Link Converters: the Current Mode Predictive Modulator," Power Electronics Specialists Conference, IEEE PESC'91, ISSN 0275- 9306, pp 268-274, USA, Junho 1991.

[13] J. Rodriguez, J. Pontt, C. Silva, P. Cortés, and S. Rees, "Predictive Current Control of a Voltage Source Inverter," 35th Annual IEEE Power Electronics Specialists Conference. Aachen, Germany, 2004.

[14] E. Wiechmann, A. Garcia, L. Salazar and J. Rodriguez, "High- Performance Direct-Frequency Converters Controlled by Predictive- Current Loop" IEEE Transactions on Power Electronics, Vol. 12, No. 3, May 1997.

[15] P. Gambôa, S. Pinto, J. Silva, E. Margato, "Predictive Optimal Control of Unity-Power-Factor Matrix Converters used in Field Oriented Controlled Induction Motor Drives", International Symposium on Industrial Electronics, Vigo, Spain, 4-7 June 2007.

[16] L. Huber, D. Borojevic, N. Burany, "Analysis, Design and Implementation of the Space-Vector Modulator for Forced-Commutated Cycloconverters" IEE Proceedings-B, Vol. 139, no 2, March 1992, pp. 103-113.

[17] J. Palma, "Accionamentos Electromecânicos de Velocidade Variável" Fundação Calouste Gulbenkian, Portugal, 1999.

[18] M. Bollen, "Understanding Power Quality Problems", Wiley- Interscience, ISBN 0-7803-4713-7.

[19]. SilvaNeto, J.; Rolim, G.; Control of a Power Circuit Interface of a Flywheel-based Energy Storage System; UFRJ, Cidade Universitiria, Rio de Janeiro, Brazil,

[20]. Jeoung, H.; Choi, J.; High Efficiency Energy Conversion and Drives of Flywheel Energy Storage System using High Temperature Superconductive Magnetic Bearings; School of Electrical and Electronics Engineering Chungbuk National University; S Korea;

[21]. Samineni, S.; Johnson, B.; Hess, H.; Law, J.; Modeling and Analysis of A Flywheel Energy Storage System for Voltage Sag Correction

[23]. Kenny, B.; Kascak, P.; Hofmann, H.; Mackin, M.; Santiago, W; Jansen, R.; Advanced Motor Control Test Facility for NASA GRC Flywheel Energy Storage System; Technology Development Unit NASA; July 2001

[24]. Dettmer, R.; Spinning Reserve; International Energy Systems; South Wirral, UK; January 1997

[25]. K. Ghedamsi, D. Aouzellag and E.M. Berkouk "Control of Wind Generator Associated to a flywheel energy Storage" Journal of Renewable Energy, Volume 33, Issue 9, September 2008, Pages 2145-2156

[26]. Guo, Zhenyu; Mu, Xiaoping; Bai, Zhifeng; Cao, Binggang "Research in control of flywheel battery" Journal of Applied Science, vol. 7, Issue 21, p.3312-3316

[27]. Gabriel.C, Mircea.M "Losses and Efficiency of a Flywheel Energy Storage System with Permanent- Magnet Synchronous Machine Associated to a Variable-Speed Wind Generator" Technical University of Cluj Napoca.

[28]. B. Wang, G. Venkataramanan, "Dynamic Voltage Restorer Utilizing a Matrix Converter and Flywheel Energy Storage", Industry Applications Conference, 2007. 42nd IAS Annual Meeting. Conference Record of the 2007 IEEE, Volume, Issue , 23-27 Sept. 2007 Page(s):208–215.

[29]. G. Zanei, E. Cevenini, H. Ruff, S. Harrison "UPS Flywheel Energy Storage System"

[30]. Michael Mathew "Design of flywheel for improved energy storage using computer aided analysis" -project report submitted to Department of Mechanical Engineering National Institute of Technology, Rourkela,

[31]. Senan M. Bashi, Norman Mariun and Ruhaizad Ishak "Development of flywheel inverter system for voltage sag mitigation" European Journal of Scientific Research ISSN 1450-216X Vol.30 No.4 (2009), pp.670-676

[32].Bjorn Bolund, Hans Bernhoff and Mats Leijon "Flywheel energy and power storage systems" Renewable and Sustainable Energy Reviews 11 (2007), 235–258

[33]. F. N. Werfel *, U. Floegel- Delor, R. Rothfeld, Riedel, D. Wippich, B. Goebel "Flywheel energy storage system (fess) with magnetic bearings" Adelwitz Technologiezentrum GmbH (ATZ), Germany

[34].Paulo Gambôa, S. Ferreira Pinto, J. Fernando Silva and Elmano Margato "A flywheel energy storage system with matrix converter controlled permanent magnet synchronous motor"

[35]. TD. Nguyen, KJ. Tseng, S. Zhang and C. Zhang, "A flywheel cell for energy storage system" ICSET 2008

[36]. http://www.nlh.nl.ca

[37]. J. Cotrell and W. Pratt, "Modeling the Feasibility of Using Fuel Cells and Hydrogen Internal Combustion Engines in Remote Renewable Energy Systems", National Renewable Energy Laboratory (NREL), 1617 Cole Boulevard, Golden, Colorado 804013393,September 2003. URL: http://www.osti.govl bridge

[38] D.A. Bechrakis, EJ. McKeogh and P.D. Gallagher, "Simulation and operational assessment for a small autonomous wind-hydrogen energy system", Energy conversion and Management, 47 (2006), pp. 46-59.

[39]. S.R. Vosen and J.O. Keller, "Hybrid energy storage systems for stand-alone electric power systems: optimization of system performance and cost through control strategies", International Journal of Hydrogen Energy, 24 (1999), pp. 139-1156.

[40]. Mohammad Saad Alam and David W. Gao, "Modeling and Analysis of a Wind/PV/Fuel Cell Hybrid Power System in HOMER", Second IEEE Conference on Industrial Electronics and Applications, 2007, pp. 1594-1599.

[41]. Baeconpower.com

[42]. https://analysis.nrel.gov/homer

[43]. http://www.{.allingrain.com/world/CA/OS/Ramea.html

[44]. Erich Hau, "Wind turbines: Fundamentals, Technologies, Application, Economics",
Springer Verlag Berlin Heidelberg New York, ISBN: 3-540-57064-0,2000.

[45]. N0l1hern Power Systems, 29 Pitman Road, Bane, VT 05641, United States. URL: www.northernpower.com

[46] Frontier Power Systems, Attn: Carl Brothers, 392 Church Street, Alberton, PEl COB I BO, Canada. Email: carl.brothers@pei.sympatico.ca

[47] S.N. Bhadra, D. Kastha, S. Baneljee, "Wind Electrical Systems", Oxford University Press, YMCA Library Building, Jai Singh Road, New Delhi 110001, ISBN-IO: 0-19567093-0, 2005.

[48] MATLAB/SIMULINK and MATLAB/SimPower Systems are the products of The MathWorks, 3 Apple Hill Drive, Natick, MA 01760-2098, USA. URL: http://www.mathworks.com

[58] Mohd. Abdus Salam, "Fundamentals of Electric Machines", Alpha Science International Ltd., 7200 The Quorum, Oxford Business Park North, Garsington Road, Oxford, OX4 2JZ, U.K., ISBN: 1-84265-275-3,2005.

[59] Seyoum, D., Rahman, M.P. and Grantham, c., "Terminal voltage control of a wind turbine driven isolated induction generator using stator oriented field control," Proceedings of the Eighteenth Annual IEEE Applied Power Electronics Conference and Exposition (APEC '03), Miami Beach (FL, USA), vol. 2, 2003, p. 846-852.

[60] Hydrogenics Canada, 5985 McLaughlin Road, Mississauga, ON, Canada L5R IB8.

[61] Licht, Stuart, "Solar Hydrogen Generation: Toward a Renewable Energy Future", Springer, 2008, ISBN: 978-0-387-72809-4.

[62] J.M. Vidueira, A. Contrerasa, T.N. Veziroglu, "PV autonomous installation to produce hydrogen via electrolysis, and its use in FC buses", International Journal of Hydrogen Energy, pp. 927- 937,28 (2003).

[63] Keliang Zhou, J.A. Ferreira, S.W.H. de Haan, "Optimal energy management strategy and system sizing method for stand-alone photovoltaic-hydrogen systems", INTERNATIONAL JOURNAL OF HYDROGEN ENERGY, pp. 477 - 89,33 (2008).

[64] Gerhard Peharz, Frank Dimroth, UrsulaWittstadt, "Solar hydrogen production by water splitting with a conversion efficiency of 18%", International Journal of Hydrogen Energy, pp. 3248 - 3252, 32 (2007).

[65] D.A. Bechrakis, EJ. McKeogh, P.D. Gallagher, "Simulation and operational assessment for a small autonomous wind-hydrogen energy system", Energy Conversion and Management, pp. 46-59,47 (2006).

[66].Kodjo Agbossou, Mohanlal Kolhe, Jean Hamelin, and Tapan K. Bose, "Performance of a Stand-Alone Renewable Energy System Based on Energy Storage as Hydrogen", IEEE TRANSACTIONS ON ENERGY CONVERSION, pp. 633-640, VOL. 19, NO.3, SEPTEMBER 2004.

[67]. P. C. Krause, "Analysis of electric machinery and drive systems", (IEEE Press, 2002).

[68]. Chapmann, S.; Electric Machinery Fundamentals; McGraw Hill International Edition; Fourth Edition; 2005

[69]. Lin. P.I.H. , Messel, E.E., "Design of a real-time rotor inertia estimation system for DC motor with a personal Computer", Instrumentation and Measurement Technology Conference, 1991. IMTC-91.

[70]. http://hyperphysics.phy-astr.edu

[71]. Sérgio Faias, Patrícia Santos, Jorge Sousa1, Rui Castro. "An Overview on Short and Long-Term Response Energy Storage Devices for Power Systems Applications"